Alkylation converts riboflavin into an efficient photosensitizer of phospholipid membranes

María José Sosa, José Luis Fonseca, Aya Sakaya, María Noel Urrutia, Gabriela Petroselli, Rosa Erra-Balsells, Matías I. Quindt, Sergio M. Bonesi, Gonzalo Cosa, Mariana Vignoni, Andrés H. Thomas

PII: S0005-2736(23)00037-8

DOI: https://doi.org/10.1016/j.bbamem.2023.184155

Reference: BBAMEM 184155

To appear in: *BBA - Biomembranes*

Received date: 22 December 2022

Revised date: 12 March 2023

Accepted date: 22 March 2023

Please cite this article as: M.J. Sosa, J.L. Fonseca, A. Sakaya, et al., Alkylation converts riboflavin into an efficient photosensitizer of phospholipid membranes, *BBA - Biomembranes* (2023), https://doi.org/10.1016/j.bbamem.2023.184155

Alkylation converts riboflavin into an efficient photosensitizer of phospholipid membranes

María José Sosa[‡,1], José Luis Fonseca[‡,1,2], Aya Sakaya[2], María Noel Urrutia[1], Gabriela Petroselli[3], Rosa Erra-Balsells[3], Matías I. Quindt[3], Sergio M. Bonesi[3], Gonzalo Cosa[2], Mariana Vignoni[1*], Andrés H. Thomas[1*]

[1] Departamento de Química, Facultad de Ciencias Exactas, Instituto de Investigaciones Fisicoquímicas Teóricas y Aplicadas (INIFTA), Universidad Nacional de La Plata (UNLP), CCT La Plata-CONICET, La Plata, Argentina.

[2] Department of Chemistry, Quebec Center for Advanced Materials (QCAM), McGill University, 801 Sherbrooke Street West, Montreal, H3A 0B8, QC, Canada

[3] CIHIDECAR-CONICET, Departamento de Química Orgánica, FCEyN, Universidad de Buenos Aires, Ciudad Universitaria, Buenos Aires, Argentina

[‡] M.J.S. and J.L.F. contributed equally to this work.

* Corresponding authors e-mails:
mvignoni@inifta.unlp.edu.ar (Mariana Vignoni)
athomas@inifta.unlp.edu.ar (Andrés H. Thomas)

ABSTRACT

A new decyl chain [-$(CH_2)_9CH_3$] riboflavin conjugate has been synthesized and investigated. A nucleophilic substitution (S_N2) reaction was used for coupling the alkyl chain to riboflavin (Rf), a model natural photosensitizer. As expected, the alkylated compound (decyl-Rf) is significantly more lipophilic than its precursor and efficiently intercalates within phospholipid bilayers, increasing its fluorescence quantum yield. The oxidative damage to lipid membranes photoinduced by decyl-Rf was investigated in large and giant unilamellar vesicles (LUVs and GUVs, respectively) composed of different phospholipids. Using a fluorogenic probe, fast radical formation and singlet oxygen generation was demonstrated upon UVA irradiation in vesicles containing decyl-Rf. Photosensitized formation of conjugated dienes and hydroperoxides, and membrane leakage in LUVs rich in poly-unsaturated fatty acids were also investigated. The overall assessment of the results shows that decyl-Rf is a significantly more efficient photosensitizer of lipids than its unsubstituted precursor and that the association to lipid membranes is key to trigger phospholipid oxidation. Alkylation of hydrophilic photosensitizers as a simple and general synthetic tool to obtain efficient photosensitizers of biomembranes, with potential applications, is discussed.

KEYWORDS:

Nucleophilic substitution; riboflavin; lipid peroxidation; LUVs; GUVs

INTRODUCTION

Oxidative stress results in lipid oxidation in many physiological and pathological processes [1,2]. Lipid oxidation triggered by electromagnetic radiation, through photosensitized reactions, contributes to the damage in the photosynthetic apparatus, food oxidation and skin photodamage. However, lipid photo-oxidation can be advantageously induced in important applications such as disinfection and photodynamic therapy (PDT) [3–5]. Photosensitized oxidations can take place through different mechanisms, grouped under type I and type II mechanisms [6,7]. In type I mechanisms, a direct reaction of the photosensitizer in an excited state, typically a triplet excited state, with the target molecule or substrate, generates radicals through electron transfer or hydrogen atom abstraction. Then, the corresponding formed radicals can be involved in a large number of competitive reactions to finally yield stable oxidized photoproducts. In type II mechanisms, an energy transfer from the triplet excited state of the photosensitizer to dissolved O_2 occurs, yielding singlet molecular oxygen ($^1O_2$) [7], a highly reactive electronically excited form of oxygen that may next react with target substrates such as unsaturated lipid. The first mechanism corresponds to contact-dependent pathways, where a direct encounter between the excited photosensitizer and the substrate occurs. The latter involves contact-independent processes, where an intermediary species, $^1O_2$, reacts with the target [8].

All unsaturated lipids, including phospholipids, glycolipids and cholesterol, can be oxidized by photosensitized processes. In cell membranes, bis-allylic hydrogens, present in poly-unsaturated fatty acids (PUFAs) of phospholipids, are the easiest positions to undergo oxidation via both types of mechanisms [9,10]. However, in contrast to non-photochemical processes, photoinduced lipid oxidation can also take place in allylic hydrogens present not only in PUFAs, but also in mono-unsaturated fatty acids (MUFAs) [11]. The first non-radical products of both type I and type II mechanisms are hydroperoxide compounds, which can easily undergo further reactions [12].

It has been suggested that the interaction of some lipophilic photosensitizers with biomembranes explains their high photodamaging capabilities [13,14]. The effect of intercalation into the membrane has been recently analyzed by comparing two PDT phenothiazium cation photosensitizers, a water soluble one and a newly prepared lipophilic one [15]. When a molecular association between the photosensitizer in its

ground state and the substrate occurs, the process is not limited by diffusion. In addition, if the excited state of the photosensitizer is not deactivated rapidly through non-radiative relaxation pathways, the photosensitization can occur much faster. On this matter, we showed that this concept readily operated in transforming water soluble pterins into highly lipophilic versions via introduction of an alkyl chain. Unconjugated oxidized pterins are a family of natural photosensitizers able to induce the photo-oxidation of different biomolecules [16,17]. Pterin (Ptr), a model hydrophilic photosensitizer of this group of compounds, does not bind to phospholipid membranes, but it induces the photo-oxidation of PUFAs present in large unilamellar vesicles (LUVs), predominantly through a type I mechanism [18]. In the search of compounds that retain the photosensitizing properties of pterins and, at the same time, are able to bind to biomembranes, a series of alkylated derivatives were synthesized by nucleophilic substitution (S_N2) reactions using 1-iododecane [19,20]. Among the decyl-pterins synthetized, due to its photochemical properties (higher intersystem crossing efficiency), 4-(decyloxy)pteridin-2-amine (*O*-decyl-Ptr) was chosen for further studies using phospholipid membranes with various compositions. The efficiency of photodamage, assessed in terms of the rates of oxidized products formation and membrane permeabilization, is much higher for *O*-decyl-Ptr than for Ptr, which indicates that the intercalation of the alkyl-pterin to the membrane enhances the photosensitized reactions [21,22]. *Mono*- and *bis*-decylated lumazines, another family of heterocyclic natural photosensitizers, have also been synthesized by nucleophilic substitution and photochemically characterized [23].

Another natural photosensitizer with similar structure to lumazines is the water-soluble vitamin B_2 (7,8-dimethyl-10-ribitylisoalloxazine) or simply, riboflavin (Rf) (Scheme 1). The photochemical behavior of Rf and other flavin derivatives are well characterized [24,25] and their photosensitizing properties have been thoroughly investigated in the context of the harmful effects of light on biological systems [26–28] as well as multiple chemical applications [28–30]. The oxidations of many biomolecules photoinduced by Rf, that predominantly operates through type I mechanism, have been studied in systems of different complexity [31–37].

In this work, we present the synthesis and structural characterization of a decyl-riboflavin conjugate (decyl-Rf), employing the same synthetic approach as that used for obtaining alkyl-pterins and alkyl-lumazines. We also describe the interaction of the new photosensitizer with lipid membranes and its photosensitizing properties on

phospholipid containing unsaturated fatty acids, using the fluorogenic probe H_4BPMHC, an α-tocopherol fluorogenic analogue that serves as a reporter of lipid peroxyl radicals as well as an indicator of singlet oxygen generation [38–43]. The results are compared to those obtained using Rf, the hydrophilic precursor. This study is aimed to contribute in the search of a simple and general synthetic tool to obtain efficient photosensitizers of biomembranes, with potential applications in PDT and photoinactivation of pathogenic microorganisms. This study, along with previous reports from our research groups (references), shows that functionalization of well-known naturally occurring hydrophilic photosensitizers, such as pterins or riboflavin, dramatically enhances the photochemical and photophysical properties of the newly generated membrane embedding analogues. This functionalization ultimately serves as a simple strategy toward enhancing the activity of photosensitizers in their application in PDT and fundamental biophysical studies of membrane properties.

EXPERIMENTAL SECTION

General

Chemicals. Riboflavin (Rf), 1-Iododecane, L-α-Soybean phosphatidylcholine (SoyPC, ≥99% (TLC), lyophilized powder), L-α-Phosphatidylcholine from egg yolk (EggPC), 5(6)- carboxyfluorescein (CF), Triton X-100, 3,5-di-tert-4-butylhydroxytoluene (BHT), xylenol orange (XO), iron (II) ammonium sulfate ($(NH_4)_2Fe(SO_4)_2.6H_2O$), sulfuric acid 98% (H_2SO_4) and Sephadex G-50 were purchased from Sigma-Aldrich. Tris-(hydroxymethyl)aminomethane (Tris) was acquired from Genbiotech. 1,2-dioleoyl-*sn*-glycero-3-phosphocholine (DOPC, powder, ≥ 99%,) was purchased from Avanti Polar Lipids Inc. *N*,*N*-dimethylacetamide (DMA), HPLC grade acetonitrile (ACN), and HPLC grade methanol (MeOH) were purchased from J.T. Baker. Dichloromethane (DCM) and chloroform-*d* were purchased from Cicarelli. Potassium carbonate (K_2CO_3) was obtained from Biopack and H_2O_2 (30%) was purchased from Merck. Water was purified using a Milli-Q® purification system.

Absorption Measurements. Electronic absorption spectra were recorded on a Shimadzu UV-1800 spectrophotometer, using quartz cells of 0.4 or 1 cm optical path length.

Synthesis, purification and characterization of a decyl chain-riboflavin conjugate

To a solution of Rf (25 mg, 0.066 mmol) in DMA (30 mL), powder potassium carbonate (9.18 mg, 0.066 mmol) was added. The mixture was sonicated and sparged with nitrogen for 20 min and then, 1-iododecane (85.48 μL, 0.398 mmol) was added. The reaction mixture was placed into an oil bath and was stirred at 70ºC for 24 h. The solution was cooled at room temperature, and the solvent was evaporated to dryness under vacuum, providing a solid residue. This solid residue was treated with a 50 mL of brine solution and then extracted with DCM (3 × 50 mL). The organic layers were combined, dried over Na_2SO_4, filtered, and evaporated to dryness. The solid obtained was purified by silica gel column chromatography (eluent: DCM 100% followed by DCM-MeOH mixtures). From the eluted fractions, a product with absorption spectrum similar to that of Rf was isolated and further purified by preparative HPLC. The final product was dried and a yellow solid was obtained.

Decyl-Rf. The solid was isolated in 12 % yield (4 mg), purity 97%. Rf (MeOH/DCM 5:95 v/v): 0.12. ^{1}H NMR (500 MHz, Chloroform-*d*) δ 8.02 (s, 1H, H-6), 7.84 (s, 1H, H-9), 4.96 – 4.87 (m, 2H, H-1'), 4.40 – 4.33 (m, 1H, H-2'), 4.04 (t, *J* = 7.2 Hz, 2H, Hα), 3.86 – 3.75 (m, 3H, H-4' and H-5'), 3.75 – 3.70 (m, 1H, H-3'), 2.52 (s, 3H, CH_3-Ar-8), 2.42 (s, 3H, CH_3-Ar-7), 1.71 – 1.64 (m, 2H, Hβ), 1.38 – 1.19 (m, 14H, H-Bulk), 0.85 (t, 3H, Hω). ^{13}C NMR (126 MHz, Chloroform-*d*) δ 160.03 (C-4), 156.60 (C-2), 149.04 (C-10a), 148.47 (C-7), 137.44 (C-8), 135.58 (C-9a), 134.96 (C-4a), 132.39 (C-5a), 132.05 (C-6), 117.01 (C-9), 73.40 (C-4'), 73.18 (C-3'), 71.39 (C-2'), 63.73 (C-5'), 48.20 (C-1'), 42.23 (Cα), 27.78 (Cβ), 32.00, 29.59, 29.57, 29.38, 29.33 27.03 and 22.70 (C-Bulk), 21.47 (Ar-CH_3), 13.45 (Ar-CH_3), 14.09 (Cω). HRMS (ESI): m/z calculated for $C_{27}H_{41}N_4O_6$ $[M+H]^+$ = 517.3026 (100%), 518.3060 (29.2%), 519.3093 (4.1%) ; m/z found 517.3031 (100%), 518.3055 (29.0%), 519.3067 (5.6%).

Nuclear magnetic resonance spectroscopy (NMR). Spectra were recorded on a Bruker Avance Neo 500 (500 MHz for ^{1}H and 126 MHz for ^{13}C). Chemical shifts (δ) are given in ppm downfield from TMS as the internal standard. Coupling constant (J) values are in Hz.

Mass spectrometry analysis. High resolution electrospray ionization (ESI) mass spectrometry (HRMS) analysis was performed in positive ion mode using the mass spectrometer BRUKER microTOF-Q II equipped with CID. Acquisition parameters: capillary temperature, 180 °C; nebulizer pressure, 0.4 Bar; capillary voltage, 4000 V; dry heater temperature, 200 °C; end plate offset voltage, −500 V; set dry gas at 4.0 L

min^{-1}; collision cell RF, 150.0 Vpp. Sample was dissolved in methanol for direct injection.

Chromatography

High-performance liquid chromatography (HPLC). A Prominence equipment from Shimadzu (solvent delivery module LC-20AT, on-line degasser DGU-20A5, communications bus module CBM-20, auto sampler SIL-20A HT, column oven CTO-10AS VP, photodiode array (PDA) detector SPD-M20A and a fluorescence (FL) detector RF-20A) was employed. Chromatographic conditions were optimized in order to determine the purity of the sample after purification, and to analyze the samples after irradiation process. The samples before and after irradiation were analyzed. A Synergi Polar-RP analytical column (ether-linked phenyl phase with polar endcapping, 150 x 4.6 mm, 4 µm, Phenomenex) was used for separation. 100 % MeOH was used as mobile phase with a flow rate of 0.3 mL min^{-1}.

Preparative High-performance liquid chromatography (P-HPLC). A Shimadzu Prominence equipment (solvent delivery module LC-20AT, communications bus module CBM-20, UV/vis detector SPD-10A, fraction collector FRC-10A and manual injector) was employed. A Synergi Polar-RP 80 Å semi-prep column (ether-linked phenyl phase with polar endcapping, 250 × 10 mm, 4µm, Phenomenex) was used for separation with 100 % MeOH as mobile phase and a flow of 1.5 mL min^{-1}.

Molecular exclusion chromatography. Sephadex G-50 was equilibrated in pure water and poured into a 0.8 × 22 cm column. Then, the column was equilibrated with Tris 20 mM buffer pH 8. Samples were eluted with the same buffer and collected in 1 ml fractions.

Fluorescence measurements

Steady-state and time-resolved fluorescence measurements were performed at room temperature using a single-photon-counting equipment FL3TCSPC-SP (Horiba Jobin Yvon), described elsewhere [44].

To obtain the fluorescence spectra, the sample solution in a quartz cell was irradiated with a CW 450W Xenon source through an excitation monochromator and the luminescence was registered at 90° with respect to the incident beam, after passing through an emission monochromator, using a room-temperature R928P detector. The

fluorescence quantum yields (Φ_F) were determined from the corrected fluorescence spectra using Equation 1:

$$\Phi_F = \Phi_F^R \frac{I/A}{I^R/A^R}\left(\frac{n^R}{n}\right)^2 \quad (1)$$

where I is the total fluorescence intensity, A is the absorbance at the excitation wavelength (λ_{exc}), n is the refractive index of each solvent and the superscript R refers to the reference fluorophore. In our experiments Rf in aqueous solution (Φ_F= 0.27) [45] was used as a reference. To avoid inner filter effects, the absorbance of the solutions, at the excitation wavelength, was kept below 0.10. Spectra were corrected for wavelength-dependent emission profiles with corrections factors supplied by the manufacturer and using the software FluorEssence™ version 3.9 (Horiba Jobin Yvon).

In time-resolved experiments, a NanoLED source (maximum at 461 nm, ~ 1 ns pulse duration) was used for excitation, and the emitted photons, after passing through a monochromator, were detected by a TBX-04 detector and counted by a FluoroHub-B module. The selected counting time window for the measurements reported in this study was 0-200 ns.

Studies performed with large unilamellar vesicles (LUVs)

Preparation of LUVs. Lipids (DOPC, EggPC and SoyPC) were dissolved in chloroform and dried under nitrogen stream to form thin lipids films, which then were hydrated with Tris buffer (10 mM, pH 8). To form LUVs, the samples were vortexed for a few minutes, followed by extrusion through a 100 nm polycarbonate membrane (Avanti Polar Lipids, Inc.). LUVs were kept at 4 °C prior to being used the same day. Dynamic light scattering measurements were performed with a Malvern Zetasizer Nano-ZS to determine the size of LUVs formed. Results showed a diameter of 1.4 (± 0.1) × 10^2 nm (mean ± SD, triplicates). The polydispersity index was 0.12.

Binding constant determination. A titration method was used to determine the binding constant (K_b) of Rf and decyl-Rf to LUVs [46]. Gradually increasing quantities of LUVs were added to a solution of the photosensitizer (2 μM) in Tris buffer. The mixture was shaken, incubated for ~15 min, and the fluorescence spectrum was recorded. Corrected fluorescence spectra obtained by excitation at 450 nm were recorded between 465 and 750 nm, and the total fluorescence intensities (F) were calculated by integration of the fluorescence band between 465 and 750 nm. K_b was

then extracted by fitting a plot of F_L as a function of lipid concentration to Equation 2 below.

$$F_L = F_0 + (F_\infty - F_0)\frac{[L]}{\frac{1}{K_b}+[L]} \quad (2)$$

where F_0, F_L and F_∞ represent the fluorescence intensity of the compound without lipid, with lipid at concentration L, and that which would be obtained asymptotically at complete binding, respectively. [L] is the concentration of lipid.

Steady-state irradiation. The continuous photolysis of compounds in air-equilibrated solutions was carried out by irradiation in quartz cells (0.4 cm optical path length). A Rayonet RPR 3500 lamp (Southern N.E. Ultraviolet Co.) with emission centered at 350 nm [band width (FWHM) 20 nm] was employed as radiation source.

FOX 2 assay. Experiments were performed according to the procedure described by Wolff with some modifications [47]. The method is based on the oxidation of ferrous ions to ferric ions by hydroperoxides (Equation 3), which react with XO to form a colored complex (Equation 4).

$$ROOH + Fe^{2+} \longrightarrow Fe^{3+} + RO^{\bullet} + OH^{-} \quad (3)$$

$$Fe^{3+} + XO \longrightarrow \text{blue-purple complex} \quad (4)$$

The reagent was prepared as follows: 250 μM $(NH_4)_2Fe(SO_4)_2.6H_2O$ (9.8 mg) and 25 mM H_2SO_4 (139 μL) were dissolved in 5 mL of H_2O, mixed with 4 mM BHT (88.2 mg), 100 μM XO (7.2 mg) and 45 mL of MeOH. Afterwards, another 45 mL of methanol and 5mL of water were added. For the experiment, aliquots of 100 μL of samples were added to 700 μL of FOX 2 reagent in microtubes, homogenized in a vortex mixer and left to react for 30 min in the dark at room temperature. After incubation, the absorbance of samples was read between 200 and 700 nm. As the extinction coefficient of Fe/XO complex may differ depending on the acid used, pH, solvents and with the nature of hydroperoxides, concentrations of lipid hydroperoxides were calculated as mM H_2O_2 equivalents based upon a standard curve spanning a 0 - 0.4 mM H_2O_2 range (R^2 0.9907), which were prepared and submitted to the same treatment of the studied samples.

Photoinduced carboxyfluorescein (CF) release. LUVs were prepared as described above, but for hydration, 500 μL of 50 mM CF in 10 mM Tris buffer (pH = 8) was used, generating a LUV suspension with CF encapsulated in the inner compartment. Free CF

was removed by exclusion chromatography in a Sephadex G-50 column (1 cm × 15 cm) in equilibrium with 0.3 M NaCl in 10 mM Tris buffer (pH = 8) and the fraction containing LUVs was collected [48]. The high CF amounts inside LUVs results in fluorescence self-quenching, therefore an increase in CF fluorescence indicates membrane damage and leakage of CF to the outer solution [49]. The final volume was 1000 µL in 0.3 M NaCl - 10 mM Tris buffer (pH = 8), adding 25 µL of lipid suspension. The concentration of photosensitizer was 5 µM, except for the control which had no compound. The irradiation was performed in a fluorescence quartz cell of 0.4 cm path length. Fluorescence spectra between 500 nm and 680 nm were monitored as function of irradiation time, with excitation at 485 nm. At the end of the experiment, Triton X-100 was added, and the fluorescence was once again recorded. The fraction of released CF was then calculated as follows:

$$\% \, CF_{released} = \frac{F - F_0}{F_T - F_0} \times 100 \qquad (5)$$

where F_0 is the initial fluorescence intensity, F is the fluorescence intensity at each irradiation time, and F_T is the total fluorescence intensity after membrane disruption with Triton X-100. The emission of Triton X-100 is negligible under the experimental conditions used.

Studies performed with giant unilamellar vesicles (GUVs)

Preparation of GUVs. GUVs were formed via the gel-assisted formation method [50]. Glass microscope slides (3"×1"×1mm) were sonicated for one hour in a piranha solution (3:1 solution of H_2SO_4 and 30% H_2O_2) followed by rinsing three times in molecular biology grade water then once in HPLC grade Acetone. A polyvinyl alcohol (PVA) polymer film was formed atop the glass slides by spreading 100 µL of a 5% (w/w) PVA solution in molecular biology grade water in a 1 cm × 2.5 cm rectangular shape. The PVA film was left to dry at 50°C for one hour. Next, a chloroform solution (< 20 µL) containing 1.96×10^{-7} mol DOPC, 4.0×10^{-9} mol DPPE-biotin, and 2.0×10^{-9} mol H_4BPMHC (redox-sensitive fluorogenic probe) [38] was spread over the dry PVA film. The film was then put under vacuum for 30 minutes to remove all traces of chloroform. A chamber was formed on top of the glass slide by fixing an O-ring around the PVA film. The chamber was then filled with 600 µL of a 0.1 M sucrose solution. GUVs were left to swell for 10 minutes and then added to an Eppendorf. The chamber was then washed with an additional 100 µL of the sucrose solution which was also

added to the Eppendorf. To image the GUVs, 100 μL of the GUV solution in sucrose was diluted with 400 μL of a 0.1 M solution of glucose inside the microscope imaging chamber, and the GUVs were left to sink to the bottom of the imaging chamber in the dark for 10 minutes. Photosensitizers were added externally from concentrated stocks either in H_2O (Rf) or MeOH (decyl-Rf).

Image acquisition. GUVs were imaged under a widefield microscopy setup using an inverted Nikon Eclipse Ti microscope equipped with a Perfect Focus System (PFS) and an oil-immersion objective (Nikon CFI SR Apochromat TIRF 100×, numerical aperture (NA) = 1.49). Samples were excited with the 488 nm and 405 nm output lasers (Agilent MLC400B Monolithic laser combiner), where the former excited the fluorogenic probe H_4BPMHC and the latter the photosensitizer. A multiband excitation filter (ZET405/488/561/647x, Chroma Technology) was used to clean up the laser beams, which were then coupled into the microscope objective using a multiband beam splitter (ZT405/488/561/647rpc, Chroma Technology). A ZET405/488/561/647m emission filter (Chroma Technology) was used to spectrally filter the fluorescence emission collected through the objective. An additional 540/80x bandpass filter (Chroma Technology) was used when monitoring emission from H_4BPMHC. Collected fluorescence emission was captured onto a 512 × 512 pixel (16 μm pixel size) region of a back-illuminated electron-multiplying charge-coupled device (EMCCD) camera (iXon X3 DU-897-CS0-#BV, Andor Technology). Resulting fluorescence movies consisted of 16-bit, 512 × 512 pixel images with an acquisition frequency of 10 frames per second. The camera and microscope were controlled using the Micro-Manager Software (Micro-Manager 1.4.13, San Francisco, CA, USA) and the NIS element software from Nikon, respectively. Image data analysis was conducted as recently reported [43]. Briefly, H_4BPMHC fluorescence intensity was extracted on a frame-by frame basis in order to extract fluorescence enhancement kinetics. To achieve this, GUV drifting over the acquisition period was first corrected using the "Align Stacks" tool from the ImageJ software (version 1.50e). Four lines were next drawn along four axes (vertical, horizontal, diagonal, and antidiagonal) over the GUV 2D-ring projection (such as the ones shown in Figure 6b), with the four lines intersecting at the center of the latter. The intensity profile along each of these four lines and over the entire image stack (i.e., for every frame) was extracted using the macro "StackProfileData". H_4BPMHC fluorescence intensity was determined by averaging the intensities of the two maxima along each of the four lines (8 points total, 2 from each line extracted from ring-line

intersections). The resulting intensity-time trajectory was then corrected for background fluorescence using an intensity-time profile extracted from a 4×4-pixel background region. Data collected with Rf as a photosensitizer could not be corrected for background scattering due to the hydrophilic nature of the photosensitizer, and the data was instead only corrected for the intrinsic camera offset.

RESULTS

Synthesis and structural characterization of decyl-riboflavin

To prepare the desired alkylated riboflavin derivative we reacted Rf with 1-iododecane in an S_N2 reaction carried out in DMA under basic conditions and heating at 70 °C for 24 h, providing a product with spectral features similar to Rf in 12 % yield. This product was isolated from the reaction mixture by column chromatography of silica gel using a mixture of DCM and MeOH (6 - 8 %) and then purified by P-HPLC using MeOH as the mobile phase. Its chemical structure was elucidated by means of 1D and 2D NMR spectroscopy and determined to be 3-decyl-riboflavin or 3-decyl-7,8-dimethyl-10-ribitylisoalloxazine (decyl-Rf, Scheme 1).

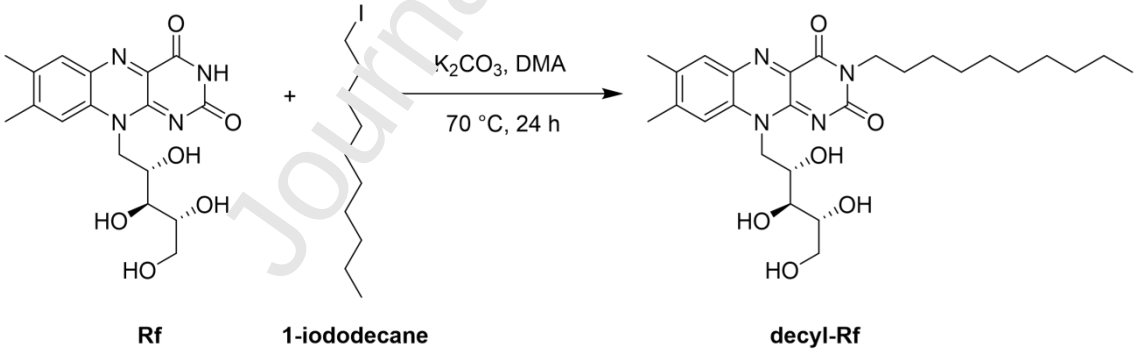

Scheme 1. Synthesis of 3-decyl-riboflavin (decyl-Rf).

The ^{1}H NMR spectrum of decyl-Rf recorded in chloroform-*d* clearly shows the characteristic signals of the α, β, bulk and ω protons of the decyl chain attached to the riboflavin moiety at 4.04, 1.71 – 1.64, 1.38 – 1.19 and 0.85 ppm, respectively (Figure S1). Likewise, the chemical shifts of the carbon atoms of the decyl chain were also observed in the ^{13}C NMR spectra ranging from 42.2 to 14.9 ppm which are typical values of aliphatic carbons (Figure S2). COSY and HSQC 2D NMR spectra of decyl-Rf

were also recorded, allowing the unambiguous characterization of the chemical structure (Figure S3 and S4). The position where the decyl chain was linked to the riboflavin moiety comes out from the accurate analysis of the HMBC experiment in the 2D NMR spectra (Figure S5). Indeed, Figure 1 shows the partial contour spectra of decyl-Rf where good correlations were observed between the signal of the α proton of the decyl chain at 4.04 ppm and the signals of the carbonyl groups, C^2 and C^4 at 156.6 ppm and 160.1 ppm, respectively. This result confirms that the decyl chain is connected to the riboflavin moiety through the nitrogen atom N^3 as can be seen through the chemical structure of decyl-Rf depicted in Figure 3, where cyan arrows point to the spectroscopic correlation. The NMR spectroscopic analysis confirms the alkylation position of Rf at the nitrogen atom N^3 which belongs to the imide group, a noticeable acid group that provides the imide anion under basic conditions and behaves as an excellent nucleophile in the S_N2 reaction between Rf and 1-iododecane.

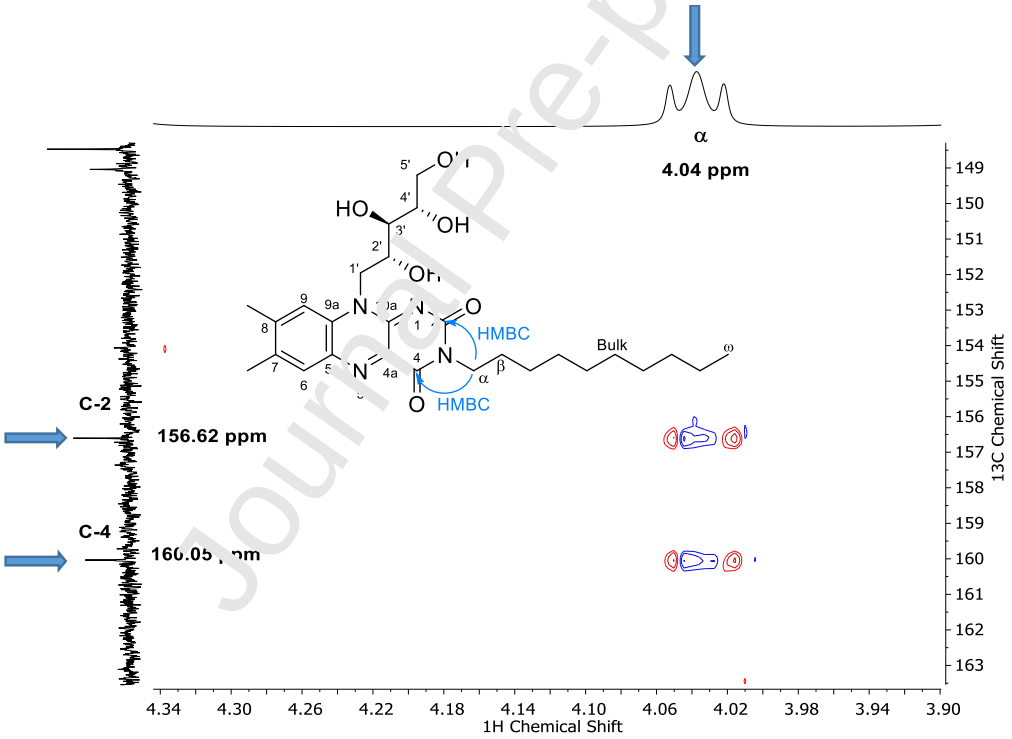

Figure 1. Partial 2D NMR HMBC (500 MHz) of decyl-Rf recorded in chloroform-*d*.

Then, the molecular weight and structure of decyl-Rf were also confirmed by HRMS. A main signal at *m/z* 517.3031 was obtained in the mass spectrum for this new product. The *m/z* value found corresponds to the protonated molecular ion, $[M+H]^+$, of a compound M bearing both Rf and the decyl moieties bonded by a sigma covalent bond ($M=[Rf\text{-}C_{10}H_{21}]$). Also, the peak corresponding to the $[M+Na]^+$ species was observed at

m/z 539.2838. Moreover, tandem mass spectrometry (MS/MS experiments, CID mode) selecting $[M+H]^+$ as precursor ion showed two diagnostic fragments; first that corresponding to the loss of the ribitol chain $C_5H_{10}O_4$ ($[M+H]^+$-$C_5H_{10}O_4$) with a peak at *m/z* 383.2437 and secondly, the one corresponding to the further loss of the decyl chain $C_{10}H_{20}$, (($[M+H]^+$-$C_5H_{10}O_4$)- $C_{10}H_{20}$) with a signal at *m/z* 243.0877 (Figures S6 and S7).

Lipophilicity, absorption and emission

Consistent with the addition of the lipophilic tail, decyl-Rf, in contrast to its hydrophilic precursor, was found to have high solubility in organic solvents (*ca.* 0.516 mg mL^{-1} in MeOH). Log*P*, the logarithmic form of the octanol/water partition coefficient, was theoretically estimated for Rf and decyl-Rf and values of -2 ± 1 and 2.5 ± 1.0 were obtained, respectively (ACD/ChemSketch Freeware).

The absorption spectrum of decyl-Rf was recorded in MeOH (Figure 2) and resulted in a very similar spectrum to that of Rf in H_2O, with four absorption bands (Table 1). Notably, spectra of solutions of decyl-Rf in H_2O showed a shoulder in the lowest energy absorption band; this effect being less pronounced at low concentrations (Figures S8 and S9). This phenomenon was explained in terms of higher hydrophobic interaction in solution, where aggregation of Rf molecules has been previously reported in concentrated aqueous solutions and in binary mixtures of organic solvents [51,52]. Here, the inclusion of long alkyl chains increases aggregation, giving rise to an excitonic band [53,54].

Similar emission spectrum, fluorescence quantum yield (Φ_F) and fluorescence lifetimes (τ_F) were also found for decyl-Rf in MeOH compared to those of Rf in H_2O, (Figure 2 and Table 1). Accordingly, the alkylation of the Rf moiety does not significantly affect the electronic distribution of the isoalloxazine ring system of Rf, which is reasonable considering the structure proposed (Scheme 1). Interestingly, in aqueous solution, the Φ_F value we determined for decyl-Rf was significantly lower than in MeOH, even though the τ_F were very similar. These findings are consistent with two fractions present in aqueous solution for decyl-Rf, an emissive one where the compound is free and a second one where decyl-Rf becomes aggregated or associated, undergoing self-quenching [53,54].

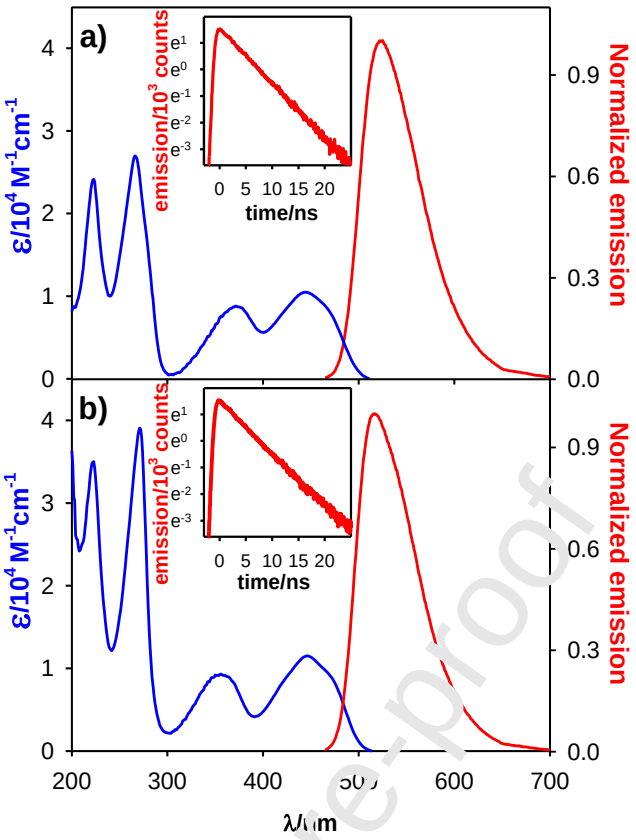

Figure 2. Absorption (blue line) and normalized emission (red line) spectra of (a) Rf in H_2O (λ_{exc}= 450 nm), (b) decyl-Rf in MeOH (λ_{exc}= 450 nm). Insets: Corresponding fluorescence decays (λ_{exc}= 461 nm, λ_{em}= 520 nm). In fluorescence measurements the concentrations was 6 μM.

Table 1. Spectroscopic properties of Rf and decyl-Rf.

		λ_{max}/nm			
compound	**solvent**	**Absorption**	**Emission**	Φ_F [a]	τ_F/ns [b]
Rf	H_2O	223/266/370/445	522	0.27±0.02	4.8±0.2
decyl-Rf	H_2O	226/275/359/453	527	0.04±0.01	4.2±0.2
	MeOH	223/271/356/446	517	0.29±0.02	5.0±0.2

[a] λ_{exc}= 450 nm; [b] λ_{exc}= 461 nm, λ_{em}= 520 nm.

Membrane binding

To investigate the interaction of Rf and decyl-Rf with phospholipid bilayers, DOPC LUVs prepared in Tris buffer and containing either compound were passed through a molecular exclusion chromatography column, using Tris as elution buffer. Fractions of 1 mL were collected and the corresponding absorption and fluorescence spectra were recorded. Relative concentrations of the photosensitizers in each fraction

were determined by integrating the emission spectra, obtained by exciting at 450 nm. LUVs were detected through their light scattering signal at 600 nm, where Rf and decyl-Rf do not absorb. The absorbance elution profiles registered for both compounds show peaks between fractions 3 and 5, associated with the elution of LUVs (Figure 3). The fluorescence elution profile obtained for Rf shows a peak between fractions 8 and 14, equal to that observed in a control performed with a solution of Rf without LUVs (Figure 3a). No fluorescence of Rf was detected at fractions where LUVs were collected, which indicates that Rf is not associated to the lipid bilayer. In contrast, decyl-Rf eluted in the same fractions where LUVs were detected (Figure 3b), which means that the alkylated compound can intercalate into the lipid membranes.

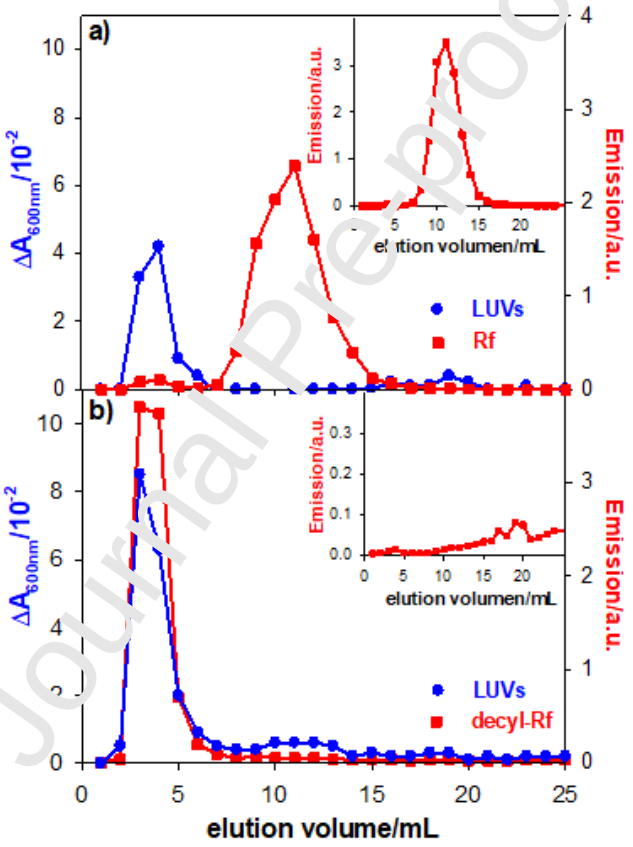

Figure 3. Elution profiles of molecular exclusion chromatography. Suspension containing DOPC LUVs (1.2 mM) and a) Rf (15 μM) or b) decyl-Rf (6 μM). Insets: controls performed with a) Rf and b) decyl-Rf in the absence of LUVs. In each fraction of 1 mL the absorbance at 600 nm (●) and the integrated fluorescence intensity by excitation at 450 nm (■) was registered to detect the LUVs and Rf/decyl-Rf, respectively.

To investigate the interaction of the photosensitizer with the lipid membranes we further conducted fluorescence imaging of single GUVs in the presence of either decyl-Rf or Rf, added to the GUVs dispersion to a final concentration of 7.5 μM. GUVs were

imaged under a widefield microscopy setup, exciting the samples at 405 nm (~12 W/cm^2). Emission was recorded between 500-580 nm, where both Rf and decyl-Rf compounds fluoresce (Figure 2). In the images registered with decyl-Rf, the membrane ring arising from the 2D projection of the 3D GUV can be seen clearly in the emission channel (Figure 4a). This result, in agreement with molecular exclusion chromatography experiments, indicates that the alkylated compound intercalates into the lipid bilayer where it emits. In contrast, images recorded under the same conditions, but using Rf instead of decyl-Rf, show no significant emission arising from the membrane (Figure 4b), thus indicating that, as expected, the hydrophilic precursor does not significantly bind to the vesicles.

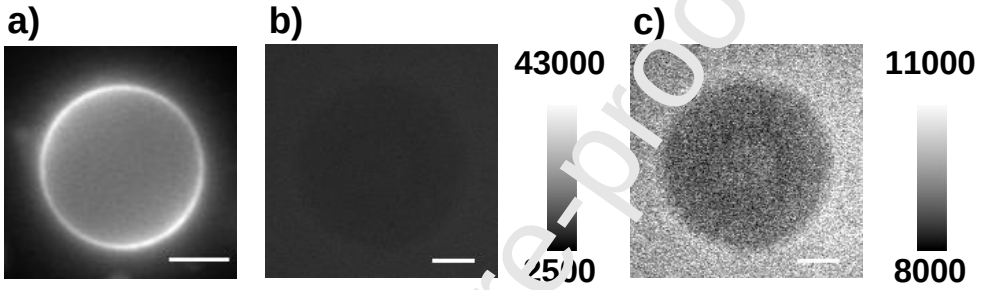

Figure 4. Fluorescence images of DOPC GUVs in suspensions containing 7.5 µM of decyl-Rf (a) or 7.5 µM of Rf (b, c). The samples were excited at 405nm (1mW) and the emission collected between 500-580 nm. Images a) and b) are displayed in the same dynamic range, while image c) corresponds to image b) depicted in a different dynamic range to better display the contrast between the inner and outer GUV emissions. The dynamic range bar is shown to the right in each case and the scale bar is 5 µm.

Choosing a reduced dynamic range, the Rf emission was observed as an increased intensity surrounding the GUV which otherwise appeared dark in its interior (Figure 4c). This observation confirms that Rf does not bind to the GUVs, while it also illustrates that the photosensitizer does not cross the lipid membranes, that is, once added to the suspension in the water phase, Rf cannot reach the inside of the vesicles.

To quantify the interaction of decyl-Rf with lipid membranes, we carried out titration curves at a constant concentration of the compound and increasing concentration of phospholipids, using EggPC LUVs. Measurements were recorded following 15 min incubation times after each addition, to ensure equilibration (no changes in intensity were recorded after 10 min). As lipid concentration increased, the emission of decyl-Rf increased to a value ~3-fold larger than the initial intensity in water (Figure 5a) and a hypochromic shift of the maximum emission wavelength was

observed (inset Figure 5a). By fitting the fluorescence intensity as a function of the concentration of EggPC, the binding constant of decyl-Rf to LUVs (K_b) was determined to be 1.4 (±0.7) × 10^4 M^{-1} (Figure 5b). Similar experiments performed with Rf did not show a significant change in the emission spectrum with the concentration of phospholipid, as expected (data not shown).

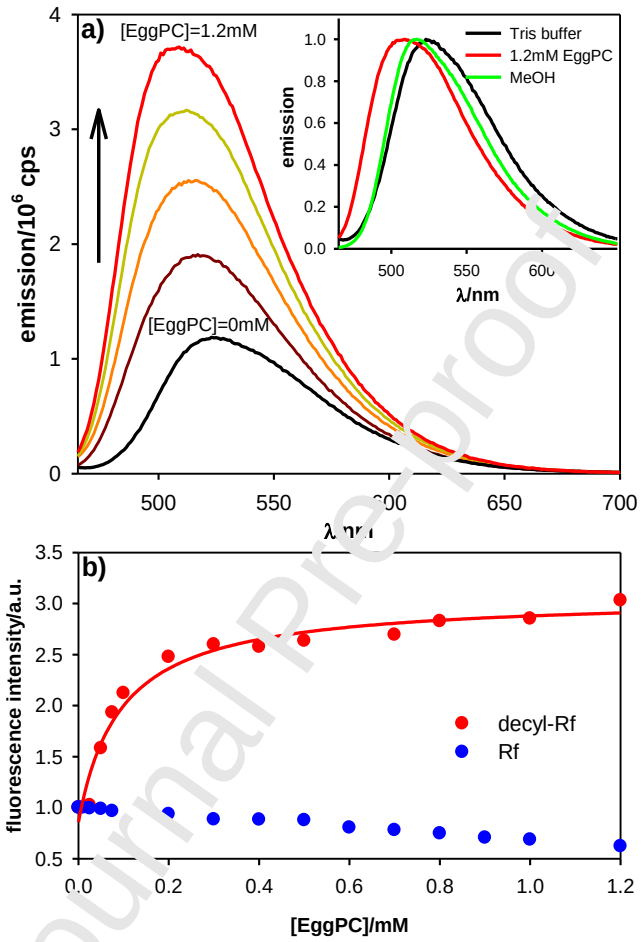

Figure 5. a) Fluorescence emission spectra of decyl-Rf (2 µM) as function of EggPC concentration (added as LUVs, arrow indicate increase in intensity with increasing EggPC concentration). Inset: Normalized fluorescence emission spectra of decyl-Rf in aqueous media (black line), lipid membranes (red line) and MeOH (green line) (λ_{exc} 450 nm). b) Titration curves: Fluorescence intensity of decyl-Rf (2 µM) (●) and Rf (2 µM) (●) as a function of the concentration of EggPC. The binding constant of decyl-Rf to EggPC LUVs was obtained by fitting the data (red line) (see Experimental Section).

Photosensitized lipid oxidation and membrane damage

To explore the oxidative damage to lipid membranes, DOPC GUVs were prepared using the fluorogenic probe H_4BPMHC [38] at a probe:lipid mole ratio of 1:100. This probe bears the chromanol moiety of α-tocopherol (trap) and a lipophilic BODIPY tail (reporter) where intramolecular photoinduced electron transfer renders the

probe non-emissive. Oxidation of the chromanol moiety (yielding H_4BPMHC_{ox}) by either lipid peroxyl radicals [55], produced via e.g. type I photoprocesses, or by singlet oxygen [43], via a type II photoprocess, restores the BODIPY emission (Figure 6c), thus providing a sensitive method to detect oxidation processes in the lipid membrane [38–43,55–57].

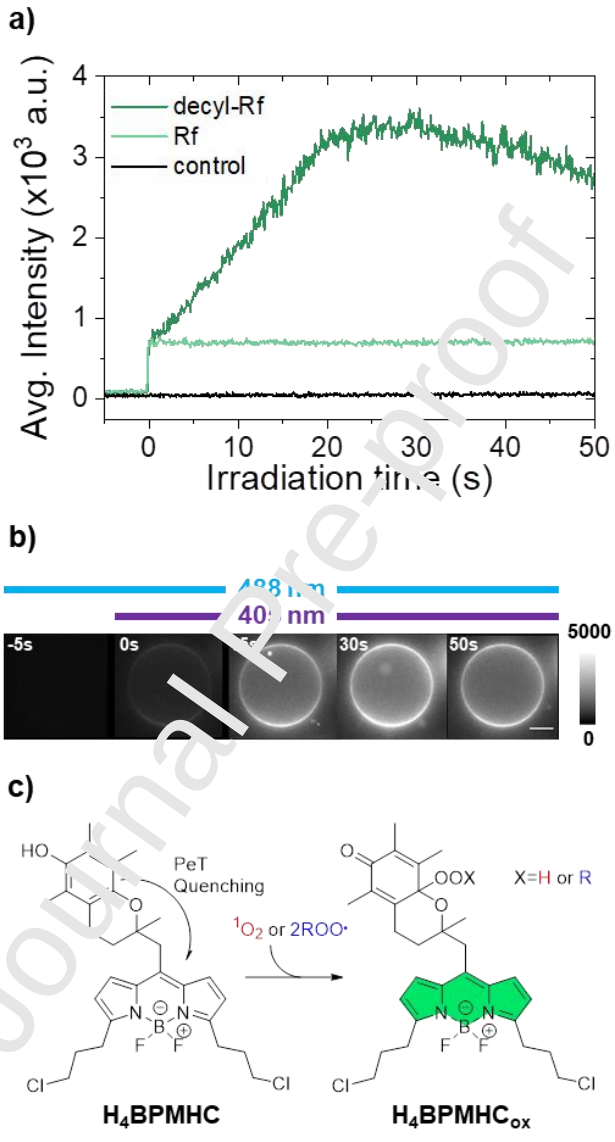

Figure 6. a) Intensity-time trajectory of H_4BPMHC embedded within GUVs and irradiated in the presence of decyl-Rf (dark green), Rf (light green), or in the absence of a photosensitizer (black). b) Film strip depicting evolution of GUV-embedded H_4BPMHC emission upon its oxidation in the presence of decyl-Rf. Film strip corresponds to data shown in a). H_4BPMHC was first excited with a 488 nm laser (5 µW) in order to determine GUV parameters prior to the start of photosensitization, which was initiated by exciting decyl-Rf or Rf with a 405 nm laser (50 µW). Ensuing generation of reactive intermediates was recorded through H_4BPMHC emission enhancement. Scale bar = 10 µm. c) Structure of H_4BPMHC and proposed oxidation product upon reaction with singlet oxygen ($^1O_2$) or other reactive oxygen species. H_4BPMHC:DOPC = 1:100. [decyl-Rf]=[Rf]=7.5 µM. t=0s corresponds to start of photosensitizer irradiation.

GUVs were imaged under a widefield microscopy setup, exciting the samples at 405 nm in the presence of decyl-Rf. The emission of H_4BPMHC was observed following its direct excitation at 488 nm and collecting its emission using a 540/80x bandpass emission filter. H_4BPMHC was monitored prior to and during the 405 nm excitation of the photosensitizers (Figure 6b). Upon 405 nm excitation in the presence of decyl-Rf, an increase in fluorescence intensity was recorded over time consistent with oxidation of membrane embedded H_4BPMHC into its emissive form H_4BPMHC_{ox} via zero order kinetics (Figure 6a-b, where we note that the first jump (within one frame) recorded at t = 0 s in the emission channel upon initiating irradiation at 405 nm is consistent with the intrinsic excitation and emission of decyl-Rf, where this emission is partly transmitted through the emission filter). No such enhancement was recorded in control experiments using either Rf as a photosensitizer or bearing no photosensitizer at all (Figure 6a). These results indicate that decyl-Rf is much more efficient than Rf in inducing lipid photo-oxidation and suggest that association to the membrane plays a key role in the photosensitizing efficiency.

The photostability of decyl-Rf was next evaluated both when free in solution and associated to lipid membranes where a suspension containing SoyPC LUVs (0.24 mM) and decyl-Rf (5 μM) in aqueous buffered pH 8 solution (Tris 10 mM) was exposed to UVA radiation. Sample irradiation was discontinued at different times, at which point the sample was diluted in MeOH to disaggregate the lipid membrane. Then the concentration of decyl-Rf was determined by chromatography. HPLC studies showed the rapid consumption of the photosensitizer upon irradiation, when membrane embedded. In turn when free in buffer solution, the half-life of decyl-Rf is observed to be ~5-fold longer under otherwise identical conditions (Figure 7).

Type I photosensitization of phospholipids is complex and involves many reactions, but the first step is always the abstraction of an allylic hydrogen from the unsaturated fatty acyl group [7]. This reaction in PUFAs leads to a lipid radical ($L^{\bullet}$) that reacts with O_2 to give a lipid peroxyl radical ($LOO^{\bullet}$), an effective chain reaction transporter [9]. In the propagation phase, the subsequent reaction of $LOO^{\bullet}$ with other PUFAs ultimately generates lipid hydroperoxides as a final product, that bear conjugated dienes. The same products are formed in the reaction of $^1O_2$ with PUFAs. This process is an “ene” reaction and with no intervention of free radical intermediates [9]. Therefore, a useful tool for an initial assessment of lipid oxidation is to investigate

the formation of hydroperoxides with conjugated dienes in vesicles rich in PUFAs.

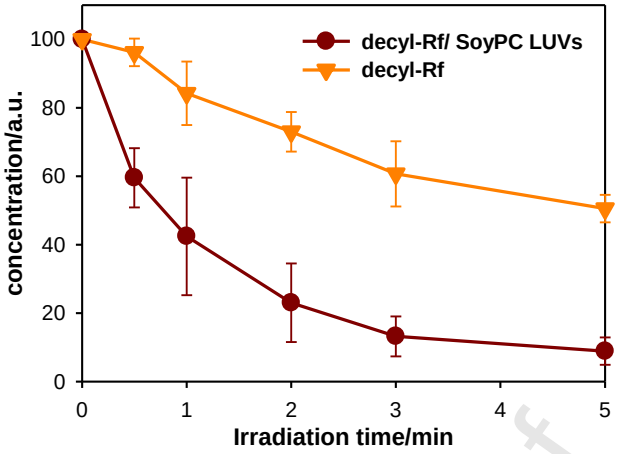

Figure 7. Time evolution of decyl-Rf concentration in aqueous solutions and in suspensions containing SoyPC LUVs under UVA irradiation. [decyl-Rf] = 5 μM, [SoyPC]= 0.24 mM, [Tris] = 10 mM, pH= 8.0.

In order to determine the extent of lipid peroxidation, the absorbance difference at 234 nm (ΔA_{234}), where conjugated dienes absorb, was monitored (Figure 8a) in experiments performed under the same conditions as those used for determining the photodegradation of decyl-Rf (Figure 7). In the time window analyzed, the appearance of the typical absorption band of the conjugated dienes, centered at 234 nm, was observed and its intensity increased with irradiation time. In this spectral region, the photosensitizer also absorbs and its absorbance is expected to change since its concentration decreases during the experiment (Figure 7). However, this fact did not interfere with the spectral analysis of the determination of conjugated dienes because the initial absorbance contribution of decyl-Rf at 234 nm is very low (< 0.06) compared to the spectral changes registered (Figure 8a). It is worth mentioning that the rate of diene formation evaluated as the slope of the plot of ΔA_{234} *vs.* irradiation time, decreased as a function of time, which is expected taking into account the consumption of the photosensitizer. A similar experiment carried out under the same conditions as above but using Rf as a photosensitizer showed smaller amounts of conjugated dienes formed (Figure 8a). A similar result was obtained in the determination of lipid hydroperoxides using the FOX 2 assay (see Experimental Section) (Figure 8b). However, in this case the difference observed between decyl-Rf and Rf was not so important as in the case of conjugated dienes.

Due to the low oxidation potential of PUFAs ($E(L^{\bullet}/LH)$), in the presence of O_2

and in the dark the oxidation takes place through thermal pathways and this process is faster if radicals have previously been generated, for example, photochemically [3,7,8]. To evaluate the contribution of the thermal oxidation in our reaction system two separate control experiments were performed with SoyPC LUVs suspensions containing decyl-Rf (same conditions of experiment of Figure 8) either in complete dark or irradiating only 7.5 min (Figure S10). While no formation of conjugated dienes was observed in the dark, a moderate increase of these products was detected after the brief irradiation time. Therefore, two assumptions can be made: (*i*) the contribution of the thermal oxidation is negligible in the time windows analyzed in Figure 8 (*c.a.* 5 min), and (*ii*) a modest light-independent lipid peroxidation continued thanks to a radical chain reaction, but only after it was photochemically triggered.

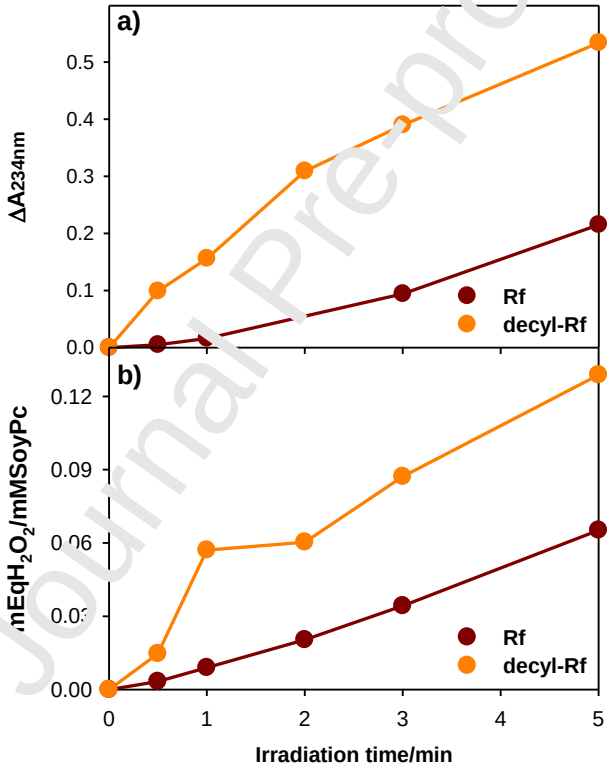

Figure 8. UVA irradiation of SoyPC LUVs suspensions ([SoyPC]= 0.24 mM) containing Rf (5 μM) or decyl-Rf (5 μM). a) Formation of conjugated dienes; b) formation of lipid peroxides determined by the FOX 2 assay.

To investigate the membrane damage generated by photosensitization in terms of membrane integrity, the CF release assay was carried out using both decyl-Rf and Rf. Here, SoyPC LUVs containing the fluorescent probe CF encapsulated under high loadings to ensure self-fluorescence quenching, were next irradiated over 30 min in the presence of either Rf or decyl-Rf photosensitizers. As shown in Figure 9, Rf produced

almost no variation in CF fluorescence during irradiation, very similar to the control without any photosensitizer. On the contrary, the emission of CF at 517 nm rapidly increased when decyl-Rf was present in LUVs, indicating that CF leakage through the membrane bilayer occurred. After 20 min of irradiation, decyl-Rf triggered leakage reached 100%, based on the fluorescence detected after the complete disruption of SoyPC LUVs by the addition of Triton X-100 (see Equation 5). At this time, controls studies with no photosensitizer or with Rf showed less than 10 % CF released. Moreover, control experiments to detect light-independent lipid peroxidation were performed stopping the irradiation after 7.5 min. As shown in the inset of Figure 9, only a slight increase in the CF fluorescence was observed when decyl-Rf is present in SoyPC LUVs, with less than 30 % CF released.

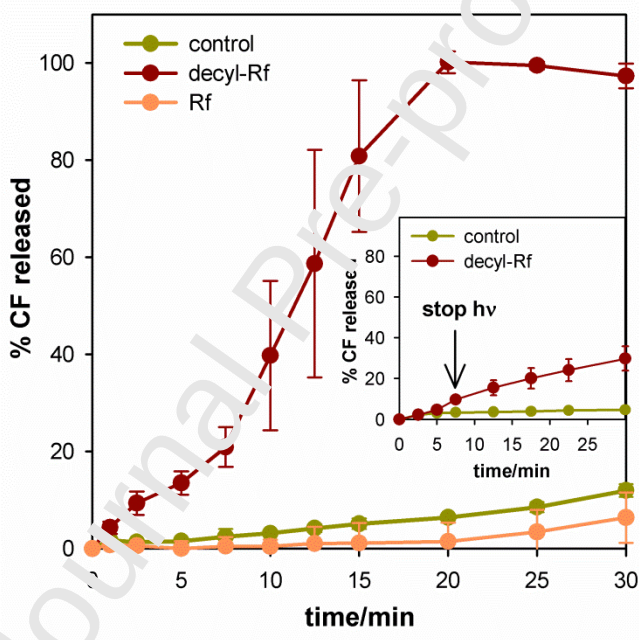

Figure 9. % CF released as a function of irradiation time using SoyPC LUVs with decyl-Rf (●), Rf (●) and without any photosensitizer (●). Error bars correspond to SD from 3 different experiments. Inset: SoyPC LUVs with decyl-Rf (●) and without any photosensitizer (●). Irradiation was stopped after 7.5 min.

DISCUSION

A new decyl chain [-$(CH_2)_9CH_3$] riboflavin conjugate has been synthesized and investigated. A nucleophilic substitution (S_N2) reaction was used for coupling a decyl chain to Rf, a model natural photosensitizer, to obtain the highly lipophilic

photosensitizer decyl-Rf (Scheme 1). It is interesting to compare the alkylation of Rf with that of related compounds. In previous studies it has been reported that decylation of Ptr and Lum only takes place on ionizable nitrogen atoms of the aromatic system or on attached phenolic groups [19,23]. In the case of Rf the two oxygen atoms at positions 2 and 4 and N^3 are suitable sites for a nucleophilic attack. However, in the case of Lum, nitrogen atoms are preferred over oxygen atoms [23]. In consequence, considering this previous information N^3 position of Rf moiety should be the most favored for reacting with 1-iododecane, which is in agreement with the assigned chemical structure of the obtained product (Figure 1).

Decyl-Rf is highly lipophilic, but it preserves the electronic structure and photophysical behavior of Rf, the hydrophilic precursor. Consequently, in contrast to Rf, decyl-Rf efficiently intercalates within phospholipid bilayers and the increase of the photosensitizer emission as a function of lipid concentration is consistent with membrane insertion and deaggregation. A ~3-fold emission enhancement was registered when decyl-Rf bound to the LUVs membrane (Figure 5), behavior that was also observed for the photosensitizer in moving from polar (H_2O) to nonpolar (hydrophobic membrane core) media. Furthermore, the hypochromic shift of the maximum emission wavelength recorded upon interaction with the lipids (inset Figure 5a) is consistent with the location of decyl-Rf in a nonpolar surrounding. Finally, the value obtained for K_b (1.4 (±0.7) × 10^4 M^{-1}) is of the same order of magnitude as those obtained for other lipophilic dyes such as xanthenes [58], porphyrins [46], and decylpterins [19].

Regarding the photosensitization studies, experiments performed using DOPC GUVs and the fluorogenic probe H_4BPMHC demonstrated that, in contrast to Rf, decyl-Rf photoinduces oxidative damage in lipid membranes (Figure 6). However, this study does not provide any information on the type of the predominant mechanism, since the probe is activated by reaction with both radicals and $^1O_2$ (Figure 6c). At this point, some experiment using a selective scavenger of $^1O_2$ might have been performed to evaluate the contribution of type II mechanism [59]. Nevertheless, we prefer to avoid this type of studies since wrong conclusions could be drawn. In fact, several scavengers are frequently used, but most of them are partial or completely hydrophilic, such as sodium azide (NaN_3), DABCO (triethylenediamine) and furfuryl alcohol, and will react with $^1O_2$ mainly present in the aqueous phase. Since in our reaction system $^1O_2$ is generated inside the lipid membrane in very close proximity to the target (double bonds of fatty acids chains), we do not trust the use of selective scavengers of $^1O_2$. In addition, the

quenching of the triplet excited state of the photosensitizer by the scavengers must also be evaluated to ensure that it reacts only with $^1O_2$, which is very challenging due to the interaction of the photosensitizer with the membrane.

However, some interesting speculations can be made on the mechanisms involved. Upon irradiation the concentration of decyl-Rf decreased faster when the compound is involved in the photosensitized process when compared to its own photochemistry (Figure 7). This is consistent with the aggregated form of decyl-Rf being self-quenched and inert to photochemical reactions. In addition, the fast photobleaching of decyl-Rf suggests the involvement of type I mechanism since the photosensitizer is usually consumed in photoinduced hydrogen abstraction reactions in lipids [60]. Finally, the predominance of type I mechanism can be inferred from the photoinduced membrane leakage studies (Figure 9). Truncated lipid- aldehydes lead to the generation of pores and consequently to the permeabilization of the membranes [3,15,21] and are formed via the β-scission reactions from alkoxyl radicals, generated in processes initiated by hydrogen abstraction [7,15].

It is interesting to consider an overall analysis of all the comparative experiments presented in the photosensitization studies. It is remarkable that whereas the photosensitizing reactivity of decyl-Rf, assessed with the fluorogenic probe (Figure 6), is strikingly higher than that of Rf, the difference in reactivity is not so important in terms of the rate of formation of photoproducts (Figure 8). This behavior, apparently contradictory, can be explained considering that hydroperoxides and conjugated dienes are reactive functional groups that can easily undergo subsequent oxidations. Therefore, although a more detailed investigation of the products formed is necessary, it can be hypothesized that decyl-Rf photoinduces the fast oxidation of the primary photoproducts, avoiding their accumulation. This hypothesis is supported by the fact that decyl-Rf affects the membrane integrity leading to leakage and permeabilization (Figure 9), while Rf does not.

CONCLUSIONS

Alkylation of the otherwise water-soluble riboflavin at position 3 rendered a highly lipophilic photosensitizer decyl-Rf that while preserving the electronic structure and photophysical/photochemical behavior of Rf, readily embeds within lipid

membranes exhibiting enhanced lipid photooxidation properties. Considering previous works with related heterocyclic compounds, such as pterins and lumazines, and the overall assessment of the results presented in this study, it can be concluded that alkylation of hydrophilic photosensitizers does not affect considerably the spectroscopic properties and the photosensitizing capability of the precursors, but it provides lipophilicity, which allows the binding of the photosensitizer to phospholipid membranes. The intercalation of the photosensitizer to the lipid bilayer increases drastically the efficiency of photosensitized oxidation processes affecting the membrane integrity and eventually leading to an increase in the permeability. The experimental data point out that alkylation of hydrophilic photosensitizers might be a simple and general synthetic tool to obtain efficient photosensitizers of biomembranes, which, in turn, might contribute to the development of new applications in photoinactivation of microorganisms and photodynamic therapy.

ACKNOWLEDGMENTS

The present work was partially supported by Consejo Nacional de Investigaciones Científicas y Técnicas (CONICET-Grant P-UE 2017 22920170100100CO), Agencia Nacional de Promoción Científica y Tecnológica (ANPCyT-Grants PICT 2015-1988, PICT 2016-1189 and PICT 2017-0925), Universidad Nacional de La Plata (UNLP-Grant 11/X840). MJS and MIQ thank CONICET for doctoral research fellowships; JLF thanks a doctoral research fellowship from ANPCyT and a DFATD fellowship from Emerging Leaders in the Americas Program (ELAP) to support his visit to Canada. GC is grateful to the Natural Sciences and Engineering Research Council (NSERC) and Canadian Foundation for Innovation (CFI) for funding. AS is thankful to the NSERC CREATE PROMOTE program for a postgraduate scholarship. MNU, GP, REB, SB, MV and AHT are research members of CONICET.

REFERENCES

[1] A.W. Girotti, Lipid hydroperoxide generation, turnover, and effector action in biological

systems, J. Lipid Res. 39 (1998) 1529–1542. http://www.scopus.com/inward/record.url?eid=2-s2.0-0031821531&partnerID=40&md5=db064898dcf09b7cb6d6f9f8ac8ab378.

[2] A. Reis, Oxidative Phospholipidomics in health and disease: Achievements, challenges and hopes, Free Radic. Biol. Med. 111 (2017) 25–37. https://doi.org/http://doi.org/10.1016/j.freeradbiomed.2017.01.014.

[3] A.W. Girotti, Photosensitized oxidation of membrane lipids: Reaction pathways, cytotoxic effects, and cytoprotective mechanisms, J. Photochem. Photobiol. B Biol. 63 (2001) 103–113. http://www.scopus.com/inward/record.url?eid=2-s2.0-0035473043&partnerID=40&md5=c3701d4350800228e3e798f2b7dc8b69.

[4] D.P. Valenzeno, Photomodification of biological membranes with emphasis on singlet oxygen mechanisms, Photochem. Photobiol. 46 (1987) 147–160. https://doi.org/10.1111/j.1751-1097.1987.tb04749.x.

[5] A. Niculescu, A.M. Grumezescu, applied sciences Photodynamic Therapy — An Up-to-Date Review, Appl. Sci. 11 (2021) 3626.

[6] M.S. Baptista, J. Cadet, P. Di Mascio, A.A. Ghogare, A. Greer, M.R. Hamblin, C. Lorente, S.C. Nunez, M.S. Ribeiro, A.H. Thomas, M. Vignoni, T.M. Yoshimura, Type I and II photosensitized oxidation reactions: Guidelines and mechanistic pathways, Photochem. Photobiol. 93 (2017) 912–919. https://doi.org/10.1111/php.12716.

[7] M.S. Baptista, J. Cadet, A. Greer, A.H. Thomas, Photosensitization reactions of biomolecules: Definition, targets and mechanisms, Photochem. Photobiol. n/a (2021). https://doi.org/https://doi.org/10.1111/php.13470.

[8] I.O.L. Bacellar, M.S. Baptista, Mechanisms of photosensitized lipid oxidation and membrane permeabilization, ACS Omega. 4 (2019) 21636–21646. https://doi.org/10.1021/acsomega.9b03244.

[9] A.W. Girotti, Photodynamic lipid peroxidation in biological systems, Photochem. Photobiol. 51 (1990) 497–509. http://www.scopus.com/inward/record.url?eid=2-s2.0-0025408177&partnerID=40&md5=1a6d6bf4ab701f6ef8f0d4242f9911b9.

[10] C. Tanielian, R. Mechin, Reaction and Quenching of Singlet Molecular Oxygen With Esters of Polyunsaturated Fatty Acids, Photochem. Photobiol. 59 (1994) 263–268. https://doi.org/10.1111/j.1751-1097.1994.tb05032.x.

[11] K.A. Riske, T.P. Sudbrack, N.L. Archilha, A.F. Uchoa, A.P. Schroder, C.M. Marques, M.S. Baptista, R. Itri, Giant Vesicles under Oxidative Stress Induced by a Membrane-Anchored Photosensitizer, Biophys. J. 97 (2009) 1362–1370. https://doi.org/10.1016/j.bpj.2009.06.023.

[12] T.M. Tsubone, M.S. Baptista, R. Itri, Understanding membrane remodelling initiated by photosensitized lipid oxidation, Biophys. Chem. 254 (2019) 106263.

https://doi.org/https://doi.org/10.1016/j.bpc.2019.106263.

[13] S. Ytzhak, S. Bernstein, L.M. Loew, B. Ehrenberg, The correlation between photosensitizers' membrane localization, membrane-residing targets and photosensitization efficiency, in: Prog. Biomed. Opt. Imaging - Proc. SPIE, 2009. http://www.scopus.com/inward/record.url?eid=2-s2.0-78649556523&partnerID=40&md5=2a03c392d7f34567abb6469401490547.

[14] G. Weber, T. Charitat, M.S. Baptista, A.F. Uchoa, C. Pavani, H.C. Junqueira, Y. Guo, V.A. Baulin, R. Itri, C.M. Marques, A.P. Schroder, Lipid oxidation induces structural changes in biomimetic membranes, Soft Matter. 10 (2014) 4241–4247. https://doi.org/10.1039/c3sm52740a.

[15] I.O.L. Bacellar, M.C. Oliveira, L.S. Dantas, E.B. Costa, H.C. Junqueira, W.K. Martins, A.M. Durantini, G. Cosa, P. Di Mascio, M. Wainwright, R. Miotto, R.M. Cordeiro, S. Miyamoto, M.S. Baptista, Photosensitized Membrane Permeabilization Requires Contact-Dependent Reactions between Photosensitizer and Lipids, J. Am. Chem. Soc. 140 (2018) 9606–9615. https://doi.org/10.1021/jacs.8b05014.

[16] C. Lorente, A.H. Thomas, Photophysics and photochemistry of pterins in aqueous solution, Acc. Chem. Res. 39 (2006) 395–402. http://www.scopus.com/inward/record.url?eid=2-s2.0-33746531697&partnerID=40&md5=fcb34ed63bfa5fee6020901aebe6ef4.

[17] C. Lorente, M.P. Serrano, M. Vignoni, M.L. Dántola, A.H. Thomas, A model to understand type I oxidations of biomolecules photosensitized by pterins, J. Photochem. Photobiol. 7 (2021) 100045. https://doi.org/https://doi.org/10.1016/j.jpap.2021.100045.

[18] A.H. Thomas, Á. Catalá, M. Vignoni, Soybean phosphatidylcholine liposomes as model membranes to study lipid peroxidation photoinduced by pterin, Biochim. Biophys. Acta - Biomembr. 1858 (2016) 139–145. https://doi.org/10.1016/j.bbamem.2015.11.002.

[19] M. Vignoni, N. Walalawela, S.M. Bonesi, A. Greer, A.H. Thomas, Lipophilic Decyl Chain–Pterin Conjugates with Sensitizer Properties, Mol. Pharm. 15 (2018) 798–807. https://doi.org/10.1021/acs.molpharmaceut.7b00136.

[20] N. Walalawela, M.N. Urrutia, A.H. Thomas, A. Greer, M. Vignoni, Alkane chain-extended pterin through a pendent carboxylic acid acts as triple functioning fluorophore, 1O2 sensitizer and membrane binder, Photochem. Photobiol. 95 (2019) 1160–1168. https://doi.org/10.1111/php.13098.

[21] M. Vignoni, M.N. Urrutia, H.C. Junqueira, A. Greer, A. Reis, M.S. Baptista, R. Itri, A.H. Thomas, Photo-oxidation of unilamellar vesicles by a lipophilic pterin: deciphering biomembrane photodamage, Langmuir. 34 (2018) 15578–15586. https://doi.org/10.1021/acs.langmuir.8b03302.

[22] A. Vignoni, C. Layana, H.C. Junqueira, A.H. Thomas, R. Itri, M.S. Baptista, M.

Vignoni, Alkylation of a hydrophilic photosensitizer enhances the contact-dependent photo-induced oxidation of phospholipid membranes, Dye. Pigment. 187 (2021) 109131. https://doi.org/https://doi.org/10.1016/j.dyepig.2020.109131.

[23] M.J. Sosa, M.N. Urrutia, P.L. Schilardi, M.I. Quindt, S.M. Bonesi, D. Denburg, M. Vignoni, A. Greer, E.M. Greer, A.H. Thomas, Mono- and bis-alkylated lumazine sensitizers: Synthetic, molecular orbital theory, nucleophilic index and photochemical studies, Photochem. Photobiol. 97 (2021) 80–90. https://doi.org/10.1111/php.13310.

[24] P.F. Heelis, The photophysical and photochemical properties of flavins (isoalloxazines), Chem. Soc. Rev. 11 (1982) 15–39. https://doi.org/10.1039/cs9821100015.

[25] M. Insińska-Rak, A. Golczak, M. Sikorski, Photochemistry of Riboflavin Derivatives in Methanolic Solutions, J. Phys. Chem. A. 116 (2012) 1199–1207. https://doi.org/10.1021/jp2094593.

[26] C.K. Remucal, K. McNeill, Photosensitized Amino Acid Degradation in the Presence of Riboflavin and Its Derivatives, Environ. Sci. Technol. 45 (2011) 5230–5237. https://doi.org/10.1021/es200411a.

[27] K. Hirakawa, T. Yoshioka, Photoexcited riboflavin induces oxidative damage to human serum albumin, Chem. Phys. Lett. 634 (2015) 221–224. https://doi.org/https://doi.org/10.1016/j.cplett.2015.06.026.

[28] R.W. Redmond, I.E. Kochevar, Medical Applications of Rose Bengal- and Riboflavin-Photosensitized Protein Crosslinking, Photochem. Photobiol. 95 (2019) 1097–1115. https://doi.org/10.1111/php.13126.

[29] D.R. Cardoso, S.H. Libardi, L.H. Skibsted, Riboflavin as a photosensitizer. Effects on human health and food quality, Food Funct. 3 (2012) 487–502. https://doi.org/10.1039/C2FO10246C.

[30] M. Wainwright, M.S. Baptista, The application of photosensitisers to tropical pathogens in the blood supply, Photodiagnosis Photodyn. Ther. 8 (2011) 240–248. https://doi.org/10.1016/j.pdpdt.2011.04.001.

[31] S. Perrier, J. Hau, D. Gasparutto, J. Cadet, A. Favier, J.-L. Ravanat, Characterization of Lysine−Guanine Cross-Links upon One-Electron Oxidation of a Guanine-Containing Oligonucleotide in the Presence of a Trilysine Peptide, J. Am. Chem. Soc. 128 (2006) 5703–5710. https://doi.org/10.1021/ja057656i.

[32] Y. Margolin, V. Shafirovich, N.E. Geacintov, M.S. DeMott, P.C. Dedon, DNA sequence context as a determinant of the quantity and chemistry of guanine oxidation produced by hydroxyl radicals and one-electron oxidants, J. Biol. Chem. 283 (2008) 35569–35578. https://doi.org/10.1074/jbc.M806809200.

[33] T. Bessho, K. Tano, S. Nishimura, H. Kasai, Induction of mutations in mouse FM3A cells by treatment with riboflavin plus visible light and its possible relation with

formation of 8-hydroxyguanine (7,8-dihydro-8-oxoguanine) in DNA, Carcinogenesis. 14 (1993) 1069–1071. https://doi.org/10.1093/carcin/14.5.1069.

[34] H. Kasai, Z. Yamaizumi, M. Berger, J. Cadet, Photosensitized formation of 7,8-dihydro-8-oxo-2'-deoxyguanosine (8-hydroxy-2'-deoxyguanosine) in DNA by riboflavin: a nonsinglet oxygen-mediated reaction, J. Am. Chem. Soc. 114 (1992) 9692–9694. https://doi.org/10.1021/ja00050a078.

[35] E. Silva, R. Ugarte, A. Andrade, A.M. Edwards, Riboflavin-sensitized photoprocesses of tryptophan, J. Photochem. Photobiol. B Biol. 23 (1994) 43–48. https://doi.org/https://doi.org/10.1016/1011-1344(93)06984-B.

[36] E. Fuentes-Lemus, M. Mariotti, J. Reyes, F. Leinisch, P. Hägglund, E. Silva, M.J. Davies, C. López-Alarcón, Photo-oxidation of lysozyme triggered by riboflavin is O2-dependent, occurs via mixed type 1 and type 2 pathways, and results in inactivation, site-specific damage and intra- and inter-molecular crosslinks, Free Radic. Biol. Med. 152 (2020) 61–73. https://doi.org/https://doi.org/10.1016/j.freeradbiomed.2020.03.004.

[37] H.-J. Wang, R. Liang, H.-H. Du, J.-X. Ai, R.-M. Han, J.-P. Zhang, L.H. Skibsted, Riboflavin and chlorophyll as photosensitizers in electroformed giant unilamellar vesicles as food models, Eur. Food Res. Technol. 243 (2017) 21–26. https://doi.org/10.1007/s00217-016-2718-3.

[38] L.E. Greene, R. Lincoln, G. Cosa, Rate of Lipid Peroxyl Radical Production during Cellular Homeostasis Unraveled via Fluorescence Imaging, J. Am. Chem. Soc. 139 (2017) 15801–15811. https://doi.org/10.1021/jacs.7b08036.

[39] K. Krumova, S. Friedland, G. Cosa, How Lipid Unsaturation, Peroxyl Radical Partitioning, and Chromanol Lipophilic Tail Affect the Antioxidant Activity of α-Tocopherol: Direct Visualization via High-Throughput Fluorescence Studies Conducted with Fluorogenic α-Tocopherol Analogues, J. Am. Chem. Soc. 134 (2012) 10102–10113. https://doi.org/10.1021/ja301680m.

[40] K. Krumova, P. Oleynik, P. Karam, G. Cosa, Phenol-Based Lipophilic Fluorescent Antioxidant Indicators: A Rational Approach, J. Org. Chem. 74 (2009) 3641–3651. https://doi.org/10.1021/jo900335z.

[41] P. Oleynik, Y. Ishihara, G. Cosa, Design and Synthesis of a BODIPY-α-Tocopherol Adduct for Use as an Off/On Fluorescent Antioxidant Indicator, J. Am. Chem. Soc. 129 (2007) 1842–1843. https://doi.org/10.1021/ja066789g.

[42] L.E. Greene, R. Lincoln, G. Cosa, Tuning Photoinduced Electron Transfer Efficiency of Fluorogenic BODIPY-α-Tocopherol Analogues, Photochem. Photobiol. 95 (2019) 192–201. https://doi.org/10.1111/php.13062.

[43] A. Sakaya, I. Bacellar, J. Fonseca, A. Durantini, J. McCain, L. Xu, M. Vignoni, A. Thomas, M. Baptista, G. Cosa, Singlet Oxygen Flux, Associated Lipid Photooxidation

and Membrane Expansion Dynamics Visualized on Giant Unilamellar Vesicles, Langmuir. 39 (2023) 442–452. https://doi.org/https://doi.org/10.1021/acs.langmuir.2c02720.

[44] M.P. Serrano, M. Vignoni, M.L. Dántola, E. Oliveros, C. Lorente, A.H. Thomas, Emission properties of dihydropterins in aqueous solutions, Phys. Chem. Chem. Phys. 13 (2011) 7419–7425. https://doi.org/10.1039/c0cp02912b.

[45] P. Drössler, W. Holzer, A. Penzkofer, P. Hegemann, Fluoresence quenching of riboflavin in aqueous solution by methionin and cystein, Chem. Phys. 286 (2003) 409–420. https://doi.org/https://doi.org/10.1016/S0301-0104(02)00969-2.

[46] N.G. Angeli, M.G. Lagorio, E.A.S. Román, L.E. Dicelio, Meso-Substituted Cationic Porphyrins of Biological Interest. Photophysical and Physicochemical Properties in Solution and Bound to Liposomes, Photochem. Photobiol. 72 (2000) 49–56. https://doi.org/10.1562/0031-8655(2000)0720049ms[pob]2.0.co2.

[47] S.P. Wolff, Ferrous ion oxidation in presence of ferric ion indicator xylenol orange for measurement of hydroperoxides, Methods Enzymol. 233 (1994) 182–189. https://doi.org/10.1016/s0076-6879(94)33021-2.

[48] R.M. Martins, R. Amino, K.R. Daghastani, I.M. Cuccovia, M.A. Juliano, S. Schenkman, A short proregion of trialysin, a pore-forming protein of Triatomainfestans salivary glands, controls activity by folding the N-terminal lytic motif, FEBS J. 275 (2008) 994–1002. https://doi.org/10.1111/j.1742-4658.2008.06260.x.

[49] J.N. Weinstein, S. Yoshikami, P. Henkart, R. Blumenthal, W.A. Hagins, Liposome-cell interaction: transfer and intracellular release of a trapped fluorescent marker, Science (80-.). 195 (1977) 489–492. https://doi.org/10.1126/science.835007.

[50] A. Weinberger, F.-C. Tsai, G.H. Koenderink, T.F. Schmidt, R. Itri, W. Meier, T. Schmatko, A. Schröder, C. Marques, Gel-Assisted Formation of Giant Unilamellar Vesicles, Biophys. J. 105 (2013) 154–164. https://doi.org/https://doi.org/10.1016/j.bpj.2013.05.024.

[51] G.K. Kasimova, S.K. Astanov, E.N. Kurtaliev, N.N. Nizomov, Structure of self-assembled riboflavin molecules in solutions, J. Mol. Struct. 1185 (2019) 107–111. https://doi.org/https://doi.org/10.1016/j.molstruc.2019.02.084.

[52] S.K. Astanov, G.K. Kasimova, E.N. Kurtaliev, N.N. Nizomov, A. Jumabaev, Electronic nature and structure of aggregates of riboflavin molecules, Spectrochim. Acta Part A Mol. Biomol. Spectrosc. 248 (2021) 119177. https://doi.org/https://doi.org/10.1016/j.saa.2020.119177.

[53] A. Niazi, A. Yazdanipour, J. Ghasemi, M. Kubista, Spectrophotometric and thermodynamic study on the dimerization equilibrium of ionic dyes in water by chemometrics method, Spectrochim. Acta Part A Mol. Biomol. Spectrosc. 65 (2006) 73–

78. https://doi.org/https://doi.org/10.1016/j.saa.2005.09.030.

[54] L. Antonov, G. Gergov, V. Petrov, M. Kubista, J. Nygren, UV–Vis spectroscopic and chemometric study on the aggregation of ionic dyes in water, Talanta. 49 (1999) 99–106. https://doi.org/https://doi.org/10.1016/S0039-9140(98)00348-8.

[55] L.E. Greene, R. Lincoln, G. Cosa, Spatio-temporal monitoring of lipid peroxyl radicals in live cell studies combining fluorogenic antioxidants and fluorescence microscopy methods, Free Radic. Biol. Med. 128 (2018) 124–136. https://doi.org/10.1016/j.freeradbiomed.2018.04.006.

[56] A. Sakaya, A.M. Durantini, Y. Gidi, T. Šverko, V. Wieczny, J. McCain, G. Cosa, Fluorescence-Amplified Detection of Redox Turnovers in Supported Lipid Bilayers Illuminates Redox Processes of α-Tocopherol, ACS Appl. Mater. Interfaces. 14 (2022) 13872–13882. https://doi.org/10.1021/acsami.1c23931.

[57] R. Godin, H.-W. Liu, G. Cosa, Ambient condition oxidation in individual liposomes observed at the single molecule level, Chem. Sci. 5 (2014) 2525–2529. https://doi.org/10.1039/C4SC00033A.

[58] I.R. Calori, D.S. Pellosi, D. Vanzin, G.B. Cesar, P.C.S. Pereira, M.J. Politi, N. Hioka, W. Caetano, Distribution of xanthene dyes in DPPC vesicles: Rationally accounting for drug partitioning using a membrane model, J. Braz. Chem. Soc. 27 (2016) 1938–1948. https://doi.org/10.5935/0103-5053.20160079.

[59] M.S. Baptista, J. Cadet, A. Greer, A.H. Thomas, Practical aspects in the study of biological photosensitization including reaction mechanisms and product analyses : A do's and dont's guide, Photochem. Photobiol. (2023). https://doi.org/10.1111/php.13774.

[60] T.T. Tasso, J.C. Schlothauer, H.C. Junqueira, T.A. Matias, K. Araki, É. Liandra-Salvador, F.C.T. Antonio, P. Homem-de-Mello, M.S. Baptista, Photobleaching Efficiency Parallels the Enhancement of Membrane Damage for Porphyrazine Photosensitizers, J. Am. Chem. Soc. 141 (2019) 15547–15556. https://doi.org/10.1021/jacs.9b05991.

Declaration of interests

☒The authors declare that they have no known competing financial interests or personal relationships that could have appeared to influence the work reported in this paper.

☐The authors declare the following financial interests/personal relationships which may be considered as potential competing interests:

Graphical abstract

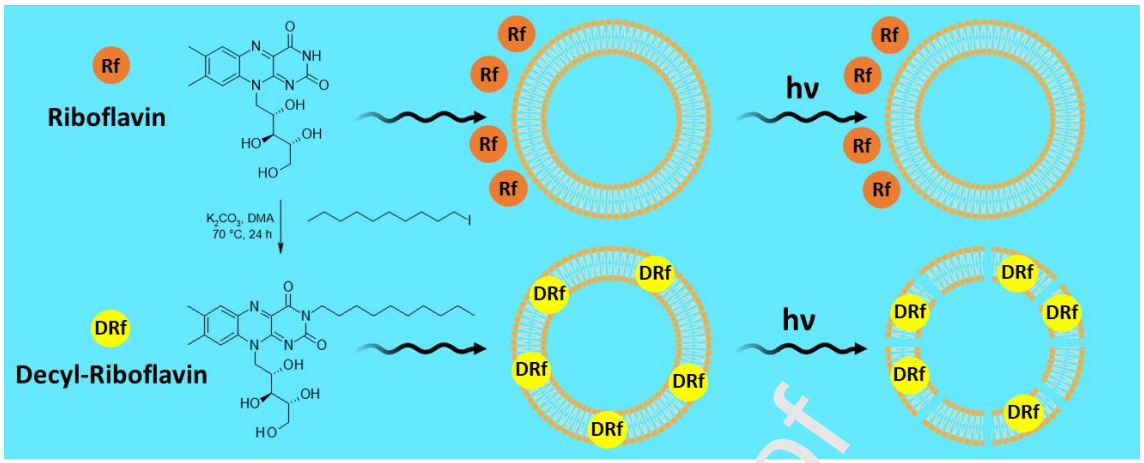

Highlights

A nucleophilic substitution was used for coupling a decyl chain to riboflavin (Rf).

The alkylated compound (decyl-Rf) is lipophilic and binds to phospholipid bilayers.

Decyl-Rf photoinduces the lipid oxidation in large and giant unilamellar vesicles.

Membrane leakage in vesicles rich in poly-unsaturated fatty acids was demonstrated.

The association to lipid membranes is key to trigger fast phospholipid oxidation.

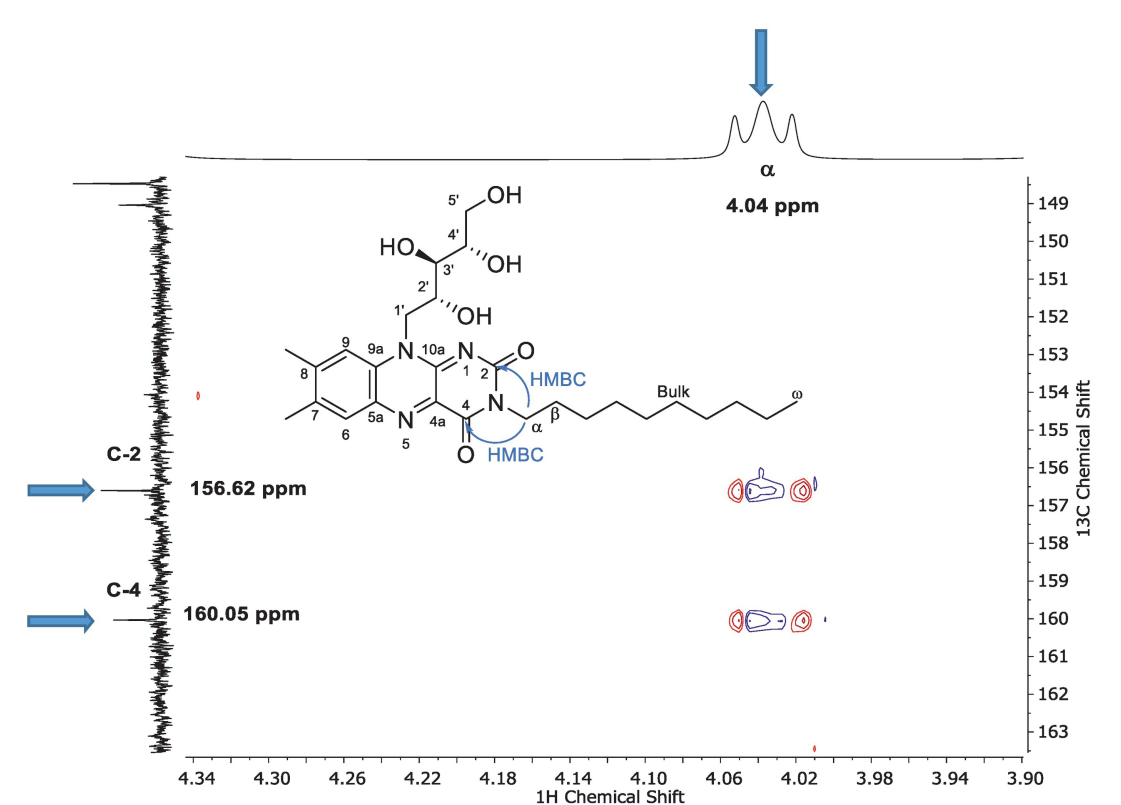
α
4.04 ppm
OH
HO
OH
OH
5'
4'
3'
2'
1'
9
9a
10a
1
2
8
7
6
5a
5
4a
4
HMBC
Bulk
ω
β
α
HMBC
C-2
156.62 ppm
C-4
160.05 ppm
4.34
4.30
4.26
4.22
4.18
4.14
4.10
4.06
4.02
3.98
3.94
3.90
1H Chemical Shift
149
150
151
152
153
154
155
156
157
158
159
160
161
162
163
13C Chemical Shift

Figure 1

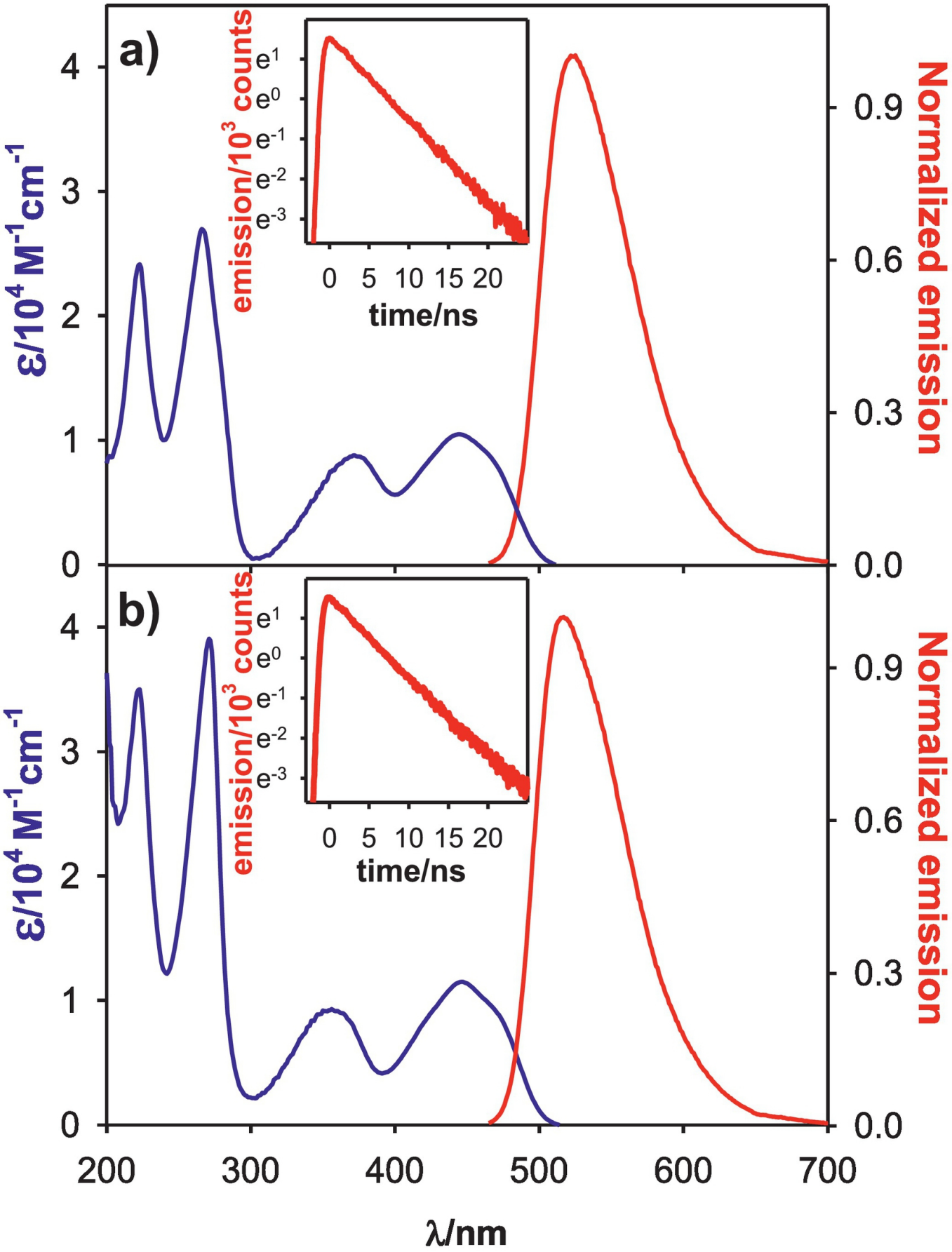
a)
b)
ε/10^4 M^-1cm^-1
emission/10^3 counts
e^1
e^0
e^-1
e^-2
e^-3
0 5 10 15 20
time/ns
Normalized emission
0 1 2 3 4
0.0 0.3 0.6 0.9
200 300 400 500 600 700
λ/nm

Figure 2

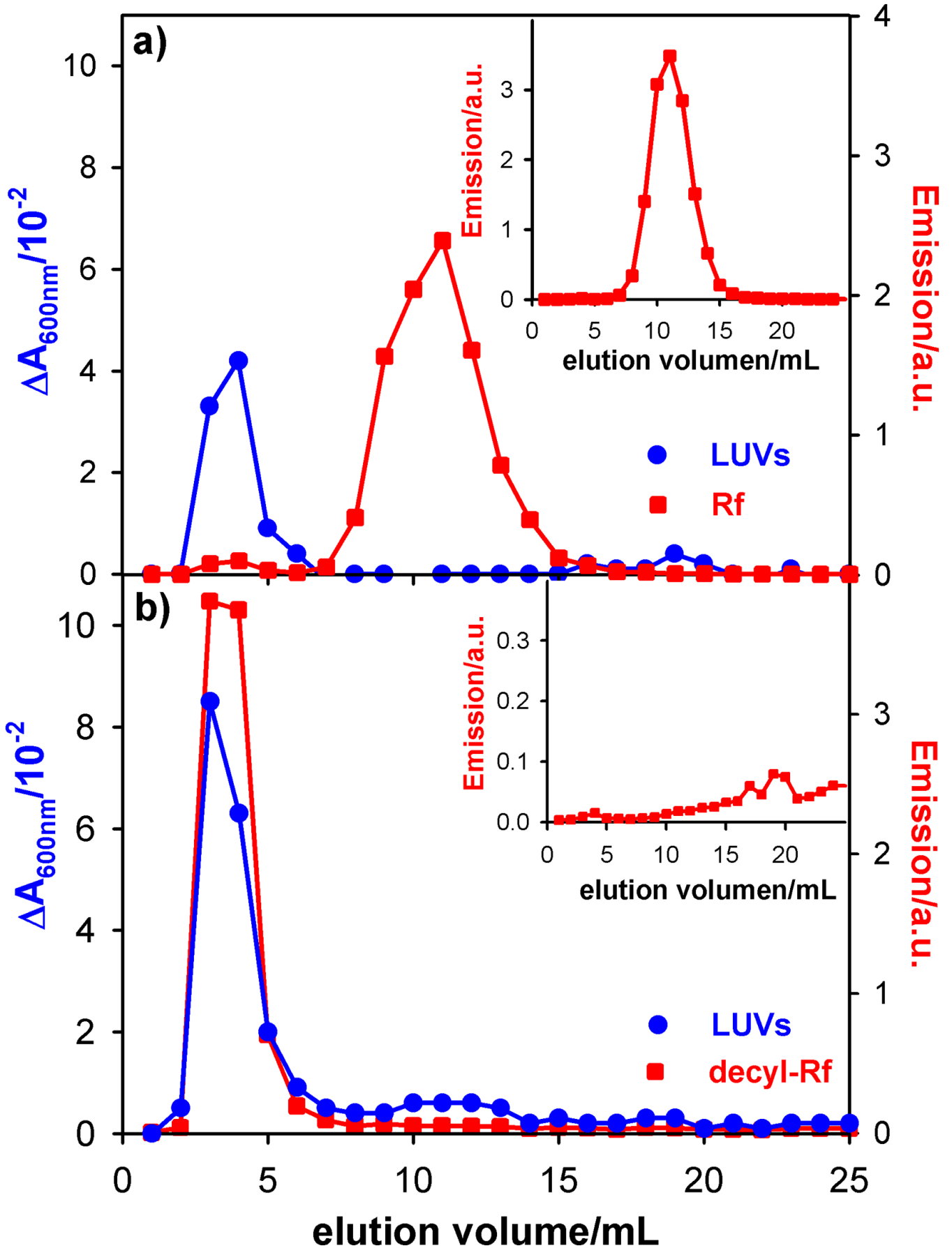
a)
b)
ΔA600nm/10-2
Emission/a.u.
elution volumen/mL
LUVs
Rf
decyl-Rf
elution volume/mL

Figure 3

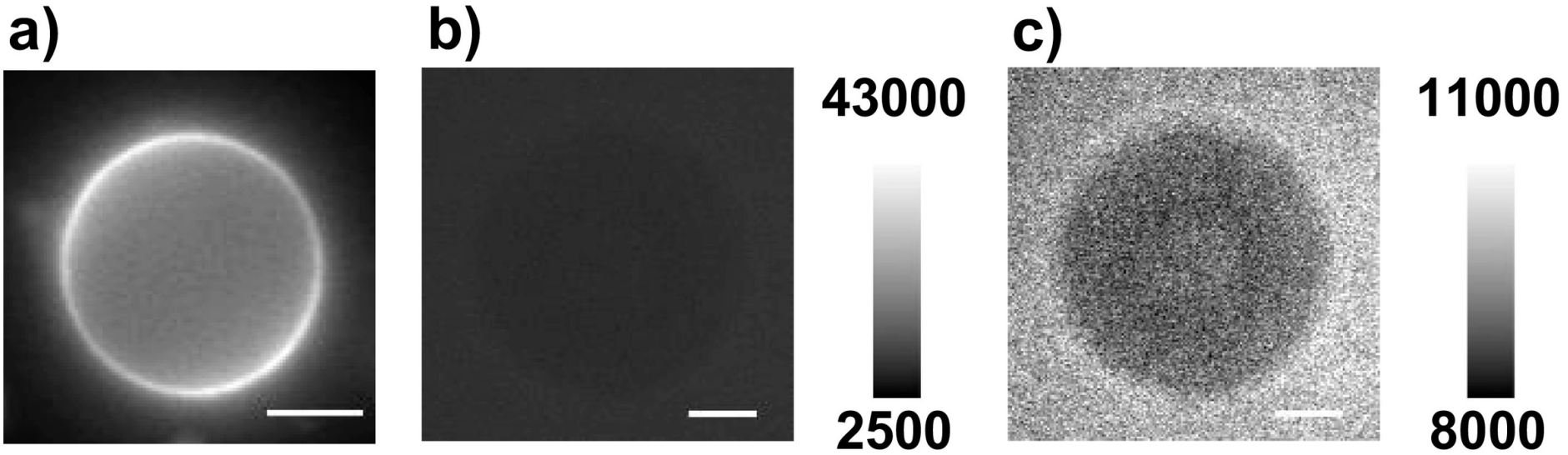

Figure 4

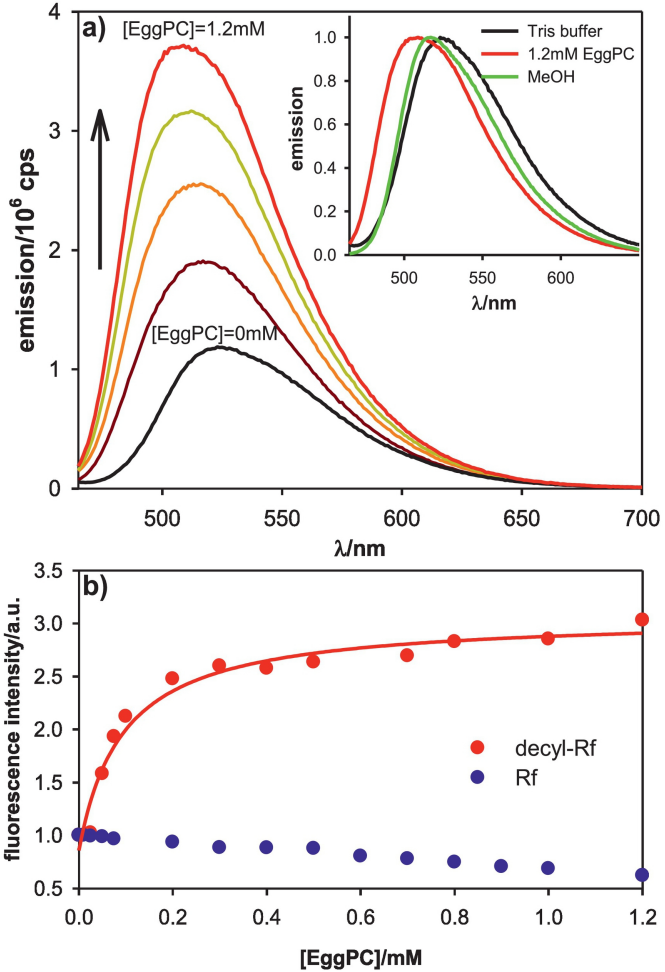
a)
[EggPC]=1.2mM
[EggPC]=0mM
emission/10^6 cps
λ/nm
Tris buffer
1.2mM EggPC
MeOH
emission
b)
fluorescence intensity/a.u.
decyl-Rf
Rf
[EggPC]/mM

Figure 5

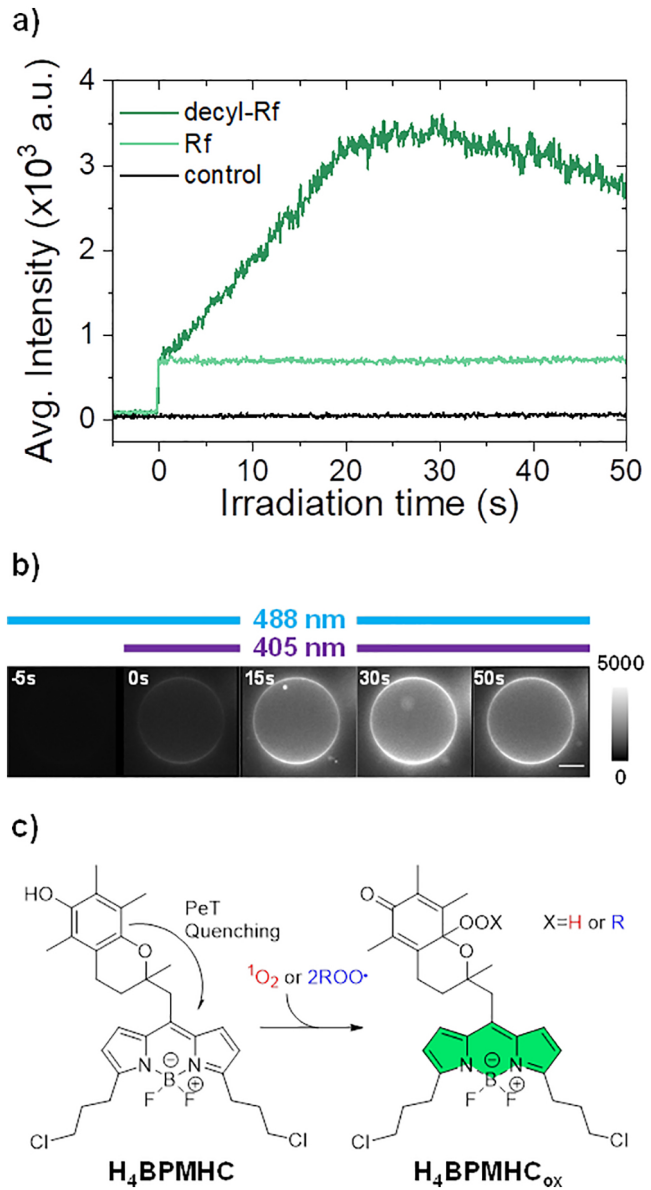
a)
Avg. Intensity (x10^3 a.u.)
decyl-Rf
Rf
control
Irradiation time (s)
b)
488 nm
405 nm
-5s
0s
15s
30s
50s
5000
0
c)
HO
PeT
Quenching
$^1O_2$ or 2ROO·
O
OOX
X=H or R
Cl
H_4BPMHC
H_4BPMHC_{ox}

Figure 6

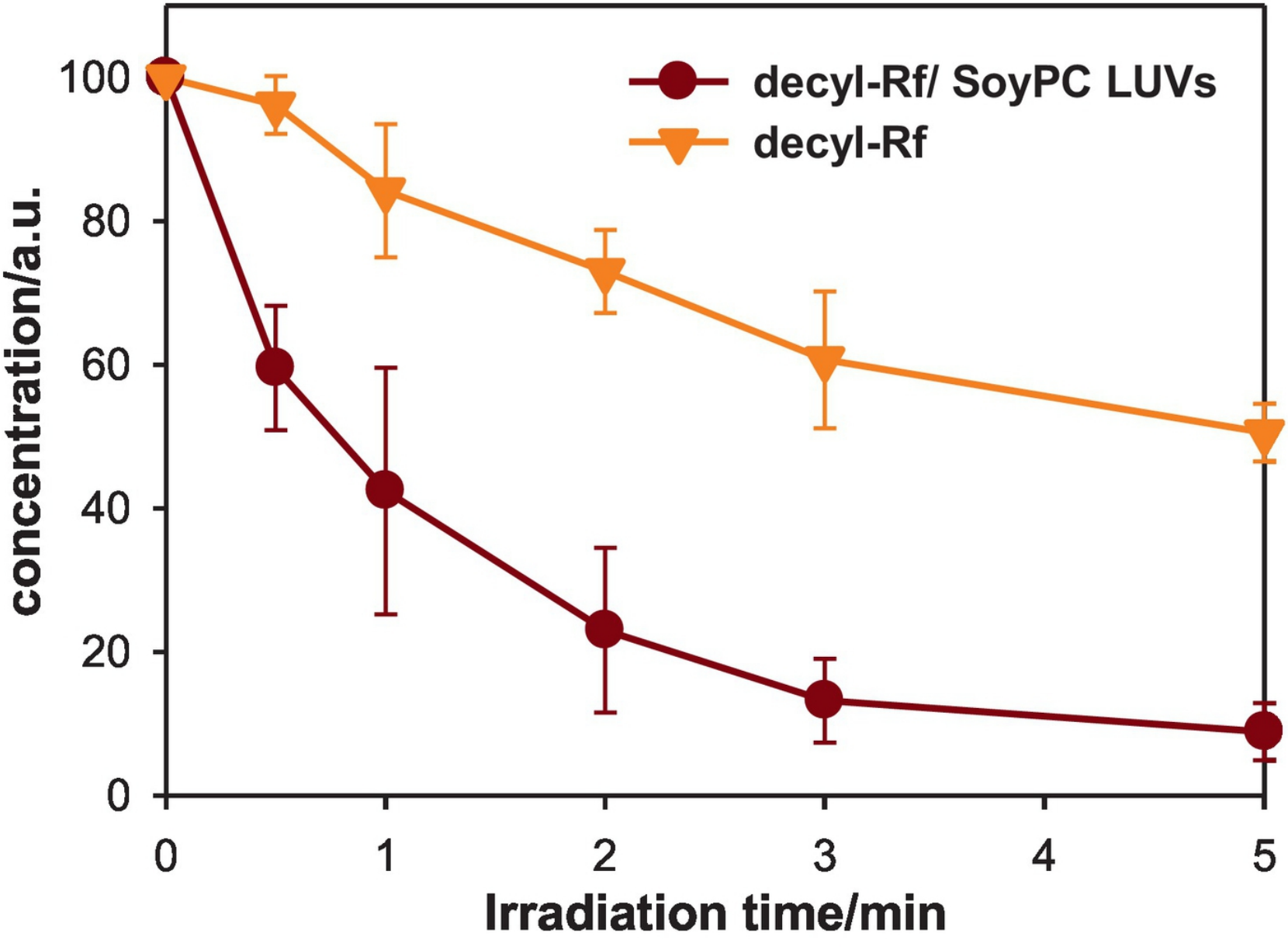
decyl-Rf/ SoyPC LUVs
decyl-Rf
concentration/a.u.
100
80
60
40
20
0
0
1
2
3
4
5
Irradiation time/min

Figure 7

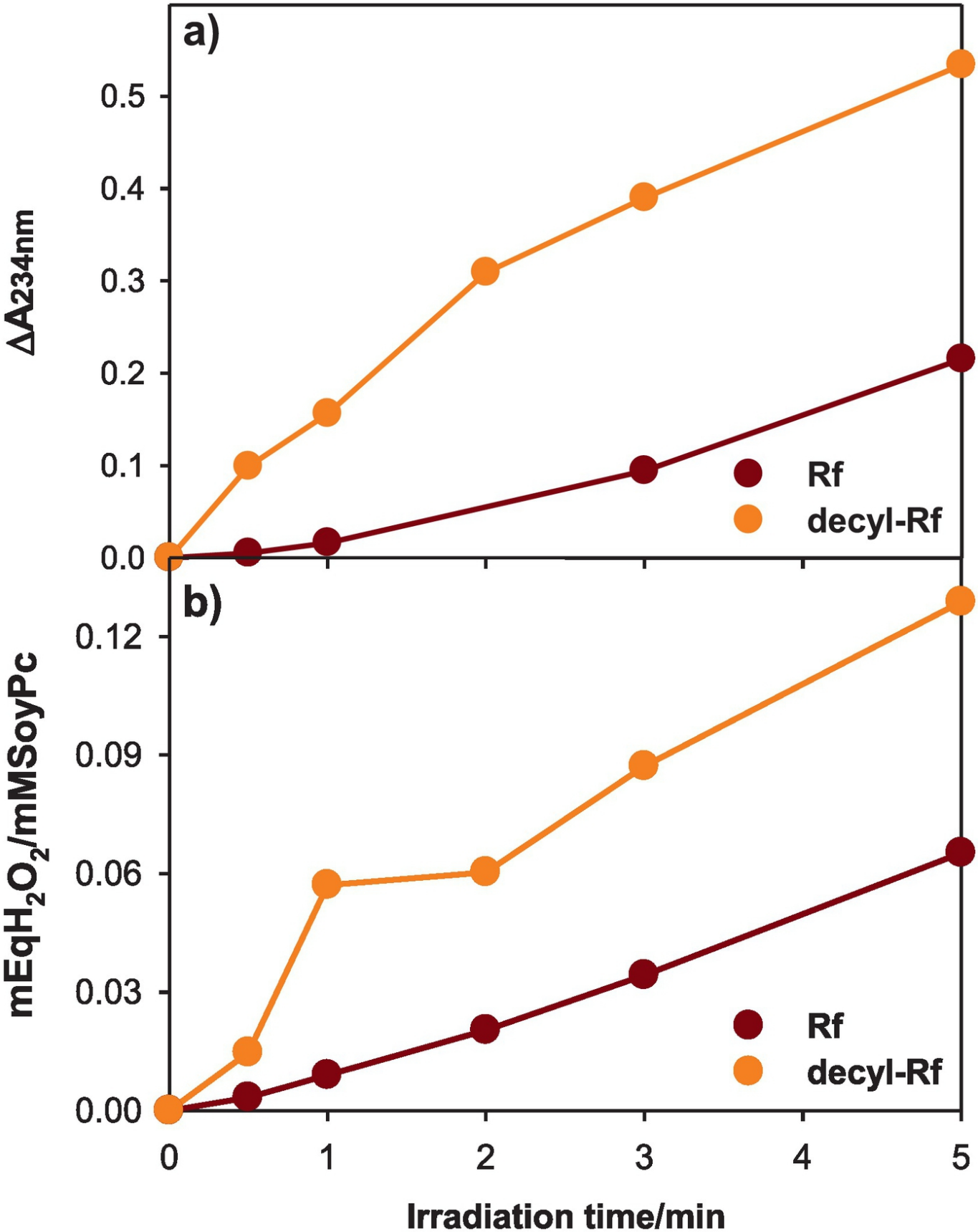
a)
0.5
0.4
0.3
0.2
0.1
0.0
ΔA234nm
Rf
decyl-Rf
b)
0.12
0.09
0.06
0.03
0.00
mEqH2O2/mMSoyPc
Rf
decyl-Rf
0
1
2
3
4
5
Irradiation time/min

Figure 8

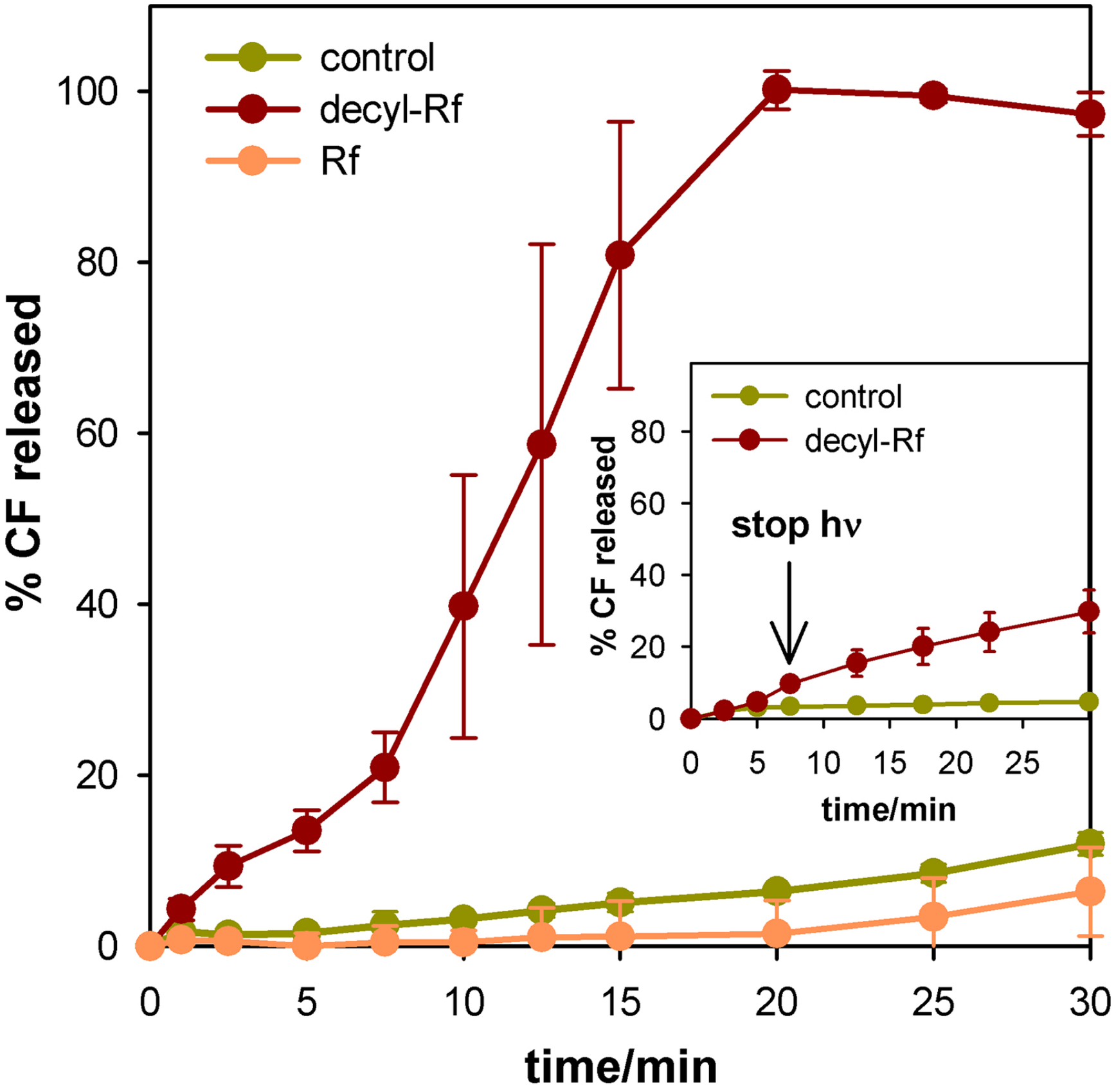

Figure 9